The export of African mineral dust across the Atlantic and its impact over the Amazon Basin

Xurong Wang[1,2,a,+], Qiaoqiao Wang[1,2,+], Maria Prass[3], Christopher Pöhlker[3], Daniel Moran-Zuloaga[3], Paulo Artaxo[4] Jianwei Gu[5], Ning Yang[1,2], Xiajie Yang[1,2], Jiangchuan Tao[1,2], Juan Hong[1,2], Nan Ma[1,2], Yafang Cheng[3], Hang Su[3], Meinrat O. Andreae[3,6]

[1.] Institute for Environmental and Climate Research, Jinan University, Guangzhou, 511443, China

[2.] Guangdong-Hongkong-Macau Joint Laboratory of Collaborative Innovation for Environmental Quality, Guangzhou, 511443, China

[3.] Multiphase Chemistry Department, Max Planck Institute for Chemistry, Mainz, 55128, Germany

[4.] Institute of Physics, University of São Paulo, São Paulo, 05508-900, Brazil

[5.] Institute of Environmental Health and Pollution Control, School of Environmental Science and Engineering, Guangdong University of Technology, Guangzhou, 510006, China

[6.] Scripps Institution of Oceanography, University of California, San Diego, CA 92093-0230, USA

[a.] now at: Atmospheric Chemistry Department, Max Planck Institute for Chemistry, Mainz, 55128, Germany

[+.] These authors contribute equally to this article

Correspondence to, Qiaoqiao Wang (qwang@jnu.edu.cn)

Abstract

The Amazon Basin is frequently influenced by the trans-Atlantic transport of African dust plumes during its wet season (January – April), which not only interrupts the near-pristine atmospheric condition in that season, but also provides nutrient inputs into the Amazon rainforest upon deposition. In this study, we use the chemical transport model GEOS-Chem to investigate the impact of the export of African mineral dust to the Amazon Basin during the period of 2013 – 2017, constrained by multiple datasets obtained from AERONET, MODIS, as well as Cayenne site and the Amazon Tall Tower Observatory (ATTO) site in the Amazon Basin. With optimized particle mass size distribution (PMSD) of dust aerosols, the model well captures observed AOD regarding both the mean value as well as the decline rate of the logarithm of AOD over the Atlantic Ocean along the transport path (AOaTP), implying the consistence with observed export efficiency of African dust along the trans-Atlantic transport. With an annual emission of 0.73 ± 0.12 Pg yr^{-1}, African dust entering the Amazon Basin has surface concentrations of 5.7 ± 1.3 μg m^{-3} (up to 15

μg m^{-3} in the northeast corner) during the wet season, accounting for 40% ± 4.5% (up to 70%) of mass concentrations of total aerosols. Observed dust peaks over the Amazon Basin are generally associated with relatively higher African dust emissions (including Sahara and Sahel) and longer lifetime of dust along the trans-Atlantic transport, namely higher export efficiency of African dust across the Atlantic Ocean. The frequency of dust events in the Amazon Basin in the wet season is around 18% averaged over the basin, with maxima over 60% at the northeast coast. During the dust events, AOD over most of the Amazon Basin is dominated by dust. Associated with dust deposition, we further estimate annual inputs of 52 ± 8.7, 0.97 ± 0.16 and 21 ± 3.6 mg m^{-2} yr^{-1} for iron, phosphorus and magnesium deposited into the Amazon rainforest, respectively, which may well compensate the hydrologic losses of nutrients in the forest ecosystem.

1 Introduction

The desert over North Africa, being the world's largest dust source, contributes to over 50% of global dust emission (Kok et al., 2021; Wang et al., 2016). Dust particles are uplifted by strong surface winds, and then typically transported downwind for a long distance, reaching Atlantic, Caribbean, America, and Europe (Prospero et al., 1981; Ben-Ami et al., 2012; Yu et al., 2019; Swap et al., 1992; Prospero et al., 2014; Wang et al., 2020). The emission varies on daily to seasonal and even decadal time scales, largely affected by local wind speed, land surface cover, soil moisture, etc (Ridley et al., 2014; Mahowald et al., 2006). Once present in the atmosphere, mineral dust can degrade air quality downwind as well as modify the atmospheric radiative balance via directly scattering and absorbing solar radiation (Ryder et al., 2013b), and altering cloud properties by acting as cloud condensation nuclei or ice nuclei (Chen et al., 1998; Demott et al., 2003; Mahowald and Kiehl, 2003; Dusek et al., 2006). Additionally, mineral dust contains iron, phosphorous, and other nutrients, and could affect ocean biogeochemistry and fertilize tropical forest upon downwind deposition (Niedermeier et al., 2014; Rizzolo et al., 2017).

There is an increased concern about the impact of African dust exerted over the Amazon basin, which being the world's largest rainforest, represents a valuable but also vulnerable ecosystem, and is sensitive to any disturbance from climate changes associated with human activities in the future (Andreae et al., 2015; Pöhlker et al., 2019). During the wet season (January – April) Amazonian aerosols are generally dominated by local biogenic aerosol, with remarkably low PM_{10} mass concentrations of a few μg m^{-3} (Andreae et al., 2015; Martin et al., 2010a; Prass et al., 2021). The near-pristine condition, however, is frequently interrupted by the transatlantic transport of African dust toward the Amazon Basin (Andreae et al., 2015; Martin et al., 2010b; Martin et al., 2010a; Talbot et al., 1990). The dusty episodes could drastically increase the aerosol optical depth (AOD, by a factor of 4), mass concentrations of coarse aerosol (with diameter > 1 μm, up to 100 μg m^{-3}), as well as crustal elements over the Amazon Basin (Ben-Ami et al., 2010; Pöhlker et al., 2019; Moran-Zuloaga et al., 2018; Baars et al., 2011; Formenti et al., 2001). Therefore, there is great interest in understanding factors controlling the export of African dust towards the Amazon Basin and the impact they might have on the environment, ecosystem, and climate.

Over the past decades, field measurements combined with satellite observation and forward/back trajectory analysis have been conducted to explore the long-range transport (LRT) of African dust toward the Amazon Basin (e.g. Ben-Ami et al., 2010; Pöhlker et al., 2018; Prospero et al., 2020). The transatlantic transport of African dust plumes is closely related to annual north-south oscillation of the intertropical convergence zone (ITCZ) (Moran-Zuloaga et al., 2018; Ben-Ami et al., 2012), favoring the path towards the Amazon Basin in the late boreal winter and spring (December-April) as the ITCZ moves southward. In addition to the annual oscillation of ITCZ, the export efficiency of African dust towards the Amazon Basin also highly depends on the lifetime of mineral dust, which is largely affected by the meteorological condition (e.g. precipitation). Dust particles are subject to wet removal when they are within or underneath precipitating clouds. For instance, Yu et al. (2020)

93 argued that El Djouf, in western Sahara, contributes more dust to the Amazon Basin
94 than the Bodélé depression as the transport paths of dust released from El Djouf are
95 less affected by the rainy cloud.
96 Besides meteorological conditions, dust size distribution can also influence its
97 lifetime and consequently the export efficiency of African dust towards the Amazon
98 Basin. Previous studies have observed that volume/mass fractions of coarse mode dust
99 particles, giant particles in particular, tend to be reduced along the transport due to
100 higher gravitational settling velocities (Ryder et al., 2018; Ryder et al., 2013b; Ryder
101 et al., 2013a; Van Der Does et al., 2016). Moreover, the optical properties of mineral
102 dust are also strongly size dependent, especially for those in sub-micron range (Liu et
103 al., 2018; Di Biagio et al., 2019; Ysard et al., 2018). For instance, Ryder et al. (2013a)
104 reported a loss of 60 − 90% of particles with diameter > 30 μm 12 h after uplift and
105 consequently an increase in the single scattering albedo from 0.92 to 0.95 associated
106 with the change in the size distribution of dust aerosols. Therefore, the size
107 distribution of dust particles is a key factor determining the efficiency of dust
108 transport and consequently the environmental and climate effect of the mineral dust
109 downwind (Mahowald et al., 2011a; Mahowald et al., 2011b).
110 It is worth mentioning that the LRT events bring not only mineral dust into the
111 Amazon Basin but also biomass burning aerosols from Africa as well as sea spray
112 aerosols (Wang et al., 2016; Holanda et al., 2020; Andreae et al., 1990; Talbot et al.,
113 1990; Ansmann et al., 2009; Baars et al., 2011), making it challenging to have a
114 quantitative assessment of the impact of African dust on the Amazon Basin. So far, a
115 few studies have attempted to quantify the impact of the LRT of African dust over the
116 Amazon Basin, but mainly focus on dust deposition only (e.g. Yu et al., 2015a; Ridley
117 et al., 2012; Yu et al., 2019). Estimates of annual dust deposition and dust deposition
118 rates into the Amazon Basin exhibit a wide range (7.7-50 Tg yr^{-1} and 0.8-19 g m^{-2} yr^{-1},
119 respectively), attributed to the application of different methods and the intrinsic
120 uncertainties associated with each method (Kok et al., 2021; Yu et al., 2015b;
121 Kaufman, 2005; Swap et al., 1992). For example, the results based on Cloud-Aerosol

Lidar and Infrared Pathfinder Satellite Observations (CALIPSO) is subject to the uncertainty associated with the Cloud-Aerosol Lidar with Orthogonal Polarization (CALIOP) extinction, vertical profile shape, dust discrimination, diurnal variations of dust transport as well as the below-cloud dust missed by CALIOP (Yu et al., 2015a). While models could be considered as a useful tool to comprehensively assess the transatlantic transport of African dust towards the Amazon Basin and the consequent impact over the Amazon Basin, there exist considerable differences among model results, attributed to the uncertainties associated with the dust parameterization in the model, including emission schemes, dust size distribution, dust deposition, etc (Kim et al.,2014; Huneeus et al., 2011; Mahowald et al., 2014). Observational constraints on the modelling results along the transport from source regions to receptor regions are thus in urgent need to accomplish a better evaluation of factors controlling the LRT of African dust and its overall impact over the Amazon Basin.

Here, we present a detailed multiyear simulation of the export of African dust across the Atlantic and its impact over the Amazon Basin (around 8.8×10^6 km^2, see Figure 1 for defined area) during 2013 − 2017 with the GEOS-Chem (chemical transport model). The aims of this study are: (1) to evaluate the model performance of dust simulation including the particle mass size distribution (PMSD), optical properties, mass concentrations as well as the export efficiency of African dust towards the Amazon Basin; (2) to analyze factors controlling the export of African dust towards the Amazon Basin; and (3) to give a comprehensive examination of the impact of African dust over the Amazon Basin, including surface aerosol concentrations, AOD and nutrient inputs upon deposition.

2 Methodology

2.1 GEOS-Chem model

2.1.1 Model overview

In this study we use the GEOS-Chem model version 12.0.0 (www. geos-chem.org) to perform a global aerosol simulation with a horizontal resolution of 2° × 2.5º. The

GEOS-Chem is driven by assimilated meteorological data GEOS-FP from the NASA Global Modeling and Assimilation Office (GMAO) (Lucchesi, 2013) with a native horizontal resolution of 0.25° × 0.3125°, which is then degraded to 2° × 2.5° for the input to GEOS-Chem. We initialize the model with a 1-year spin-up followed by an aerosol simulation from 2013 to 2017.

The aerosol simulation is an offline simulation for aerosol tracers including black carbon (BC), organic aerosols (OA), and sulfate-nitrate-ammonium aerosols in fine mode ($\leqslant$ 1 μm in diameter), sea salt in both fine and coarse (> 1 μm in diameter) modes, and mineral dust in four size bins covering the size range of 0.2 – 12 μm in diameter. Aerosol optical properties used for aerosol optical depth (AOD) calculation are mainly based on Global Aerosol Data Set (Koepke et al., 1997), with modifications in aerosol size distributions (Jaeglé et al., 2011; Drury et al., 2010; Wang et al., 2003a; Wang et al., 2003b), hygroscopic growth factor of organic aerosols (Jimenez et al., 2009), and the refractive index of dust (Sinyuk et al., 2003). AOD in the model is then calculated online at selected wavelengths assuming lognormal size distributions of externally mixed aerosols and accounts for hygroscopic growth (Martin et al., 2003).

Wet deposition in GEOS-Chem, based on the scheme of Liu et al. (2001), accounts for scavenging in both convective updrafts and large-scale precipitation. Further updates by Wang et al. (2011) are also applied, accounting for ice/snow scavenging as well as the impaction scavenging in convective updrafts. Dry deposition in the model follows the standard resistance-in-series scheme by Wesely (2007), accounting for turbulent transfer and gravitational settling (Wang et al., 1998; Zhang et al., 2001).

2.1.2 Dust emission and PMSD schemes in the model

The emission of mineral dust is based on the dust entrainment and deposition (DEAD) mobilization scheme of Zender et al. (2003) in the GEOS-Chem model. The DEAD scheme calculates the total vertical dust flux based on the total horizontal saltation flux (Q_s) using the theory of White (1979). The Q_s depends mainly on the surface wind friction velocity and the threshold friction velocity, which is determined by soil

type, soil moisture content, and surface roughness. For more details of the DEAD scheme, readers are referred to Duncan Fairlie et al. (2007).

Freshly emitted dust particles are divided into four size bins in GEOS-Chem: 0.1 − 1.0 μm, 1.0 − 1.8 μm, 1.8 − 3.0 μm, and 3.0 − 6.0 μm in radius. The first size bin is further divided into four sub-bins (0.1 − 0.18 μm, 0.18 − 0.3 μm, 0.3 − 0.6 μm, and 0.6 − 1.0 μm in radius) for the calculation of optical properties. While total dust emissions are not affected, optical properties, atmospheric lifetime and downwind concentrations of dust particles are sensitive to different PMSD schemes. Table 1 shows 3 different PMSD schemes tested in this study: V12, V12_C and V12_F. Scheme V12, which is derived based on scale-invariant fragmentation theory (Kok, 2011) with modification in tunable parameters (Zhang et al., 2013), is a default set in GEOS-Chem. However, this scheme has been only evaluated for US/Asian dust, not for Africa. On the other hand, V12_C was used in older versions of GEOS-Chem and constrained from aircraft measurements during the Saharan Dust Experiment (Ridley et al., 2012; Highwood et al., 2003). In addition, we derived V12_F based on the measurements during the Fennec aircraft observations also focusing on Saharan dust. Among all the three PMSD, V12_C has the largest mass fraction in the first bin (relatively small particles) and the lowest fraction in the last bin (large ones). In contrast, V12_F has the most dust distributed in the last bin (~ 70%) and only a little (around 5%) in the first bin (0.1 − 1.0 μm). Simulated mass extinction efficiency (MEE, also shown in Table 1) at wavelength of 550 nm for dust particles in the first sub-bin (0.1 − 0.18 μm) is 3.13 $m^2 g^{-1}$ and decreases to 0.16 $m^2 g^{-1}$ for those in the last bin (3.0 − 6.0 μm). The lifetime of dust aerosols against deposition are 5.1, 2.2, 1.7 and 0.86 d in the four bins (from small to large size), respectively. Therefore, although with the same emission, total dust AOD, lifetime, and downwind concentrations could vary greatly with PMSD upon emissions. In this study, we will evaluate these three PMSD schemes and the impact on AOD, dust concentrations as well as its export efficiency along the trans-Atlantic transport from Africa to the Amazon Basin.

2.2 Observations

The study uses observations from multiple datasets obtained from AERONET, MODIS, as well as Cayenne site and the Amazon Tall Tower Observatory (ATTO) site to constrain model results regarding the simulation of the dust export from Africa to the Amazon Basin. Table 2 summarizes these observations, including the parameters, the spatio-temporal coverage, and the corresponding application in the model. The daily data of AOD (at wavelength of 675 nm) and particle volume size distribution (PVSD) from AERONET level 2.0 (aeronet.gsfc.nasa.gov/new_web/download_all_v3_ aod.html, last access on Jun. 22, 2021(Dubovik et al., 2002)) during the year of 2013 − 2017 is used in the study to evaluate dust emissions and its PMSD over the source regions in Africa in the model. The PVSD data provided by AERONET is a column-integrated aerosol volume size distribution and with a size range of 0.05 − 15.0 μm. It is then converted to PMSD using the same densities as in the model. Only sites with valid data accounting for more than 30% of the total are considered in this study. In addition, to minimize the influence of aerosols other than dust, only data dominated by dust (simulated dust contribution to column-integrated aerosols mass concentrations > 95%) is used for the comparison of PMSD. There are a few sites not far from the coast and could be influenced by sea salt. With the above data screening, the sea salt contribution to total aerosol mass is less than 0.5%. For the comparison of AOD, the criterion is less stringent to have more data points available and uses data dominated by coarse aerosols (the contribution of fine aerosol to total aerosol volume < 3%). This criterion does not exclude sea salt and the contribution of sea salt to AOD could be up to 30% at the Capo_Verde site (22.9° W,16.7° N) over the east of the Atlantic Ocean.

The study also uses observed PMSD over central Sahara during Fennec Campaign (africanclimateoxford.net/projects/fennec/, last access: 22 June 2021) for the comparison with AERONET and our model results. Aiming to investigate dust microphysical and optical properties, 42 profiles of size distribution (0.1 − 300 μm in diameter) over both the Sahara and the Atlantic Ocean, were sampled from in-situ aircraft measurements during Fennec campaign. For more detailed description of the

aircraft measurements, readers are referred to Ryder et al. (2013a).

In addition to AERONET AOD data, level 3 daily AOD (at wavelength of 550 nm) data from the moderate resolution imaging spectroradiometers (MODIS) installed on Terra and Aqua platforms (https://ladsweb.modaps.eosdis.nasa.gov/archive/allData/61/, last access: 22 June 2021) is applied in the study to evaluate the trans-Atlantic transport of dust plumes from Africa toward Amazon Basin. For comparison, we degraded the original horizontal resolution of MODIS data (1° × 1°) to 2° × 2.5°, consistent with the model outputs.

Finally, daily PM_{10} mass concentrations during wet season (from January to April) in 2014 measured at Cayenne, French Guiana (52.3097° W, 4.9489° N, located in the northeast coast of the Amazon Basin, https://doi.org/10.17604/vrsh-w974, marked in Figure 1) and long-term aerosol measurements at the Amazon Tall Tower Observatory, Brazil (ATTO, 59.0056° W, 2.1459° S, located in central Amazon Basin, also marked in Figure 1) are used in this study to further evaluate the model performance regarding the influence of the LRT of African dust over the Amazon Basin. The measurement at Cayenne site is carried out on a cooperative basis by personnel of ATMO-Guyane, a non-profit organization. The PM_{10} samples are measured by a Taper Element Oscillating Microbalance (TEOM, model 1400 series, ThermoFisher Scientific) and then are returned to Miami for analysis (Prospero et al., 2020). Readers are referred to Prospero et al. (2020) for detailed description of the site and the data. The ATTO site was established in 2012 for the long-term monitoring of climatic, biogeochemical, and atmospheric conditions in the Amazon rainforest. Detailed description of the site and the measurements there could be found in Andreae et al. (2015). In this study, we only use the particle number size distribution from an Optical Particle Sizer (OPS, TSI model 3330; size range of 0.3 – 10 μm in diameter, divided into 16 size bins) and a Scanning Mobility Particle Sizer (SMPS, TSI model 3080, St. Paul, MU, USA; size range of 10 – 430 nm in diameter, divided into 104 size bins) over the period from 2014 to 2016. The number size distribution is

converted to mass concentrations assuming spherical particles with a constant density of 1.5 g cm^{-3} (Pöschl et al., 2010).

3 Model evaluation

Here we evaluate three different PMSD schemes regarding the model performance of dust simulation through the comparison with observed mass size distribution of column-integrated aerosol over Africa, AOD over both Africa and the Atlantic Ocean, as well as PM_{10} and dust concentrations in the Amazon Basin. Figure 2 shows the mass fractions of column-integrated aerosols retrieved from AERONET sites compared with model results based on different PMSD schemes. The location of the selected AERONET sites with valid data are marked in Figure 1 as purple symbols (including asterisks and circles). The mean mass fractions for each bin from AERONET data are 17%, 27%, 38%,17%, respectively. The comparison indicates the model results based on V12_C agrees better with the observations, with much smaller mean absolute deviation (MAD) of 2.8, followed by 4.2 for V12 and 18 for V12_F. In other words, the model results with other PMSD schemes (V12_F in particular) greatly underestimate the mass fractions in the first bin and overestimate the mass fractions in the last bin. During the Fennec campaign, the aircraft sampled two strong Saharan dust outbreaks with AOD up to 1.1, which may be associated with strong winds favoring the uplift of large particles.

Figure 3 shows the times series of daily AOD at wavelength of 675 nm during the year of 2013 − 2017 from both AERONET and model results. The locations of the selected AERONET sites with valid data over northern Africa are shown in Figure 1 as purple circles. The Capo_Verde site over the east of the Atlantic Ocean is also included to show the model performance over the ocean in addition to the land. Although different PSD schemes have little influence on the correlation between AERONET and model results with most *r* around 0.6 − 0.7, the normalized mean bias (NMB) has been significantly improved in V12_C, with a range of -12% − 11% (vs. -33% − -11% and -42% − -19% for V12 and V12_F, respectively). The severe

underestimation in AOD from V12 and V12_F could be attributed to their relatively higher dust fractions distributed in larger size bins with lower MEE.

In addition, we also compare the spatial distributions of simulated AOD over the Atlantic Ocean with MODIS AOD (at 550 nm) averaged over 2013 − 2017 in Figure 4a-d. There is a clear decreasing trend in MODIS AOD along the trans-Atlantic transport from Africa towards South America. Although all simulations show similar spatial distributions with declining trends of AOD along the transport, the results from V12_C are the most consistent with MODIS data with the highest *r* of 0.89 and the smallest NMB of 6.5% among the three schemes (vs. *r* of 0.85 and 0.81 and NMB of -13% and -19% for V12 and V12_F, respectively). Note that the model results based on V12_C tends to overestimate MODIS AOD over Africa while no significant systematic bias is found between V12_C and AERONET AOD. Wang et al. (2016) sampled MODIS data at AERONET sites over Africa and found that MODIS retrieval underestimate AERONET AOD at most sites with NMB of -12% − -36%, which partly explain the large difference between model V12_C and MODIS AOD.

Assuming first-order removal of aerosol along the transport, we could derive the removal rates of aerosols, estimated as the gradient of the logarithm of AOD (log(AOD)) against the distance over the Atlantic Ocean along the transport path (AOaTP, 20° − 50° W and 5° S − 25° N, Figure 4e). The decline rate of MODIS log(AOD) is 0.019 ± 0.0025 degree^{-1}. A similar decline rate of 0.019 ± 0.0029 degree^{-1} is found for simulated log(AOD) based on V12_C. In contrast, simulations with V12 and V12_F exhibit relatively steeper slopes of 0.021 ± 0.0040 and 0.021 ± 0.0041, respectively, implying too much aerosol removal and thus lower export efficiency along the transport. To specify the impact of different PMSD on the export efficiency of dust aerosols towards the Amazon Basin, Figure 4f also shows simulated dust AOD (DOD) along the transect from 20° to 50° W. The DOD from V12_C decreases from 0.15 ± 0.018 to 0.049 ± 0.088 along the transport, with a decreasing rate of 0.016 ± 0.0014 degree^{-1}. In contrast, DOD decreases from 0.097 ± 0.012 to 0.028 ± 0.085 with a slope of 0.018 ± 0.0016 for V12 and decreases from 0.080 ± 0.090 to 0.025 ± 0.084

with a slope of 0.017 ± 0.0014 for V12_F.

Lying in the trade wind belt, Cayenne has been taken as the gate of African dust. Hence, the comparison between simulated and observed dust concentrations at Cayenne site could evaluate model performance in reproducing the arrival of African dust to the Amazon Basin. As shown in Figure 5a, the simulation from V12_C shows excellent agreement between simulated dust and observed PM_{10} concentration during wet season, with *r* around 0.85 and NMB of -39%. The correlation from the other two simulations is similar ($r = 0.86$), but the corresponding NMB is much larger (-57% for V12 and -80% for V12_F). Based on the regression line between observed concentrations of PM_{10} and dust at the same site, Prospero et al. (2020) obtained a regional background value of PM_{10} ranging from 17 to 22 μg m^{-3}, largely attributed to sea salt aerosol, and a value of 0.9 for the slope, suggesting PM_{10} values above this range as a proxy for advected dust. Consistent with their results, the regression line between simulated dust and PM_{10} from V12_C in this study shows a background value of PM_{10} around 23 μg m^{-3}, with a value of the slope around 1.0, and the dust contribution to PM_{10} is around 53% ± 20%. In contrast, the regression lines from V12 and V12_F are much steeper, with the slope of 1.4 and 2.1, respectively, and the dust contributions are relatively smaller, 44% in V12 and 34% in V12_F.

We also compare simulated dust concentrations with observed coarse particles at ATTO site in central Amazon in wet season during 2014 – 2016 in Figure 5b. The correlation between observed and simulated data are similar for different PMSD schemes with *r* of 0.63 − 0.65. But the bias of V12_C is negligible (NMB = -0.27%) while both V12 and V12_F tend to underestimate the coarse aerosol concentrations with NMB of -36% and -55%, respectively. The dust contribution to coarse aerosols in above 80% in V12_C, but less than 70% in V12_F. This again implies relatively higher export efficiency of African dust aerosols towards the Amazon Basin with V12_C associated with their relatively higher dust fractions distributed in smaller size bins.

Overall, compared with V12 and V12_F schemes, model results based on V12_C are

more consistent with the multiple observed data sets, including column-integrated particle size distribution, AOD and surface coarse aerosol concentrations obtained either over sources or downwind of the sources. Therefore, we use the model results from V12_C (hereinafter referred to as model results unless noted otherwise) to investigate the transatlantic transport of dust from Africa and its impact over the Amazon Basin in the following sections.

4 Results and discussion

4.1 Dust emissions

Figure 1 shows the spatial distribution of simulated dust emissions and Table 3 lists seasonal and annual dust emissions in northern Africa (17.5° W − 40° E, 10° N − 35° N) for the period of 2013 − 2017. Simulated annual dust emission from northern Africa is 0.73 ± 0.12 Pg yr^{-1}, contributing more than 70% of the global dust emission (0.99 ± 0.20 Pg yr^{-1}). The result is in the range of 0.42 − 2.05 Pg yr^{-1} reported by Kim et al. (2014), who evaluated five AeroCom II global models regarding the dust simulation over similar regions.

There exists a strong seasonality in the dust emission from northern Africa, peaking in spring and winter (up to 1.2 Pg yr^{-1}) and reaching the minimum in fall (around 0.33 Pg yr^{-1}) in general. Previous studies have also pointed out that dust emissions over different African regions show distinct variations (Bakker et al., 2019; Shao et al., 2010), attributed to differences in geographical properties (Knippertz et al., 2007), vegetation cover (Mahowald et al., 2006; Kim et al., 2017), and meteorological mechanisms on a local scale (Alizadeh-Choobari et al., 2014; Wang et al., 2017; Roberts and Knippertz, 2012). Consequently, there exists substantial seasonal change in dust source regions. For instance, during boreal winter, the Bodélé Depression in northern Chad is found to be the most active triggered by the Harmattan winds, while the northwestern African dust sources become less active in contrast with the condition in boreal summer (Ben-Ami et al., 2012; Prospero et al., 2014). Therefore, we further analyze the emission variability over five different source regions in

northern Africa (Figure 1 and Table S1). On an annual basis, the contribution to total northern African dust emission is the largest from Region A (west Sahara, 36% ± 4.0%), followed by Region D (central Sahel including the Bodélé Depression, 21% ± 4.7%), Region B (central Sahara, 13% ± 2.6%), Region C (east Sahara, 12% ± 1.0%), and Region E (west Sahel, 6.5% ± 0.64%). The emission fluxes, however, are the most intensive in Region D, up to 11 ± 2.1 g $month^{-1}$ m^{-2} and are generally below 5 g $month^{-1}$ m^{-2} over the other regions.

Concerning the seasonality, higher dust emission tends to occur in boreal spring and winter, with the largest emission flux of 19 ± 4.7 g $month^{-1}$ m^{-2} from Region D. As shown in Figure 6 and S1, the emissions peak in boreal spring for Region A, B and C, but in winter for Region D and E. There is also a secondary peak in summer emissions for Region E. Correlation analysis between dust emissions and meteorological variables suggests that the seasonality is mainly driven by high surface wind speeds (with *r* of 0.79-0.96 and 0.68-0.97 for the 75^{th} and 95^{th} percentiles of 10-m wind speeds, respectively). Apparent negative correlation is also found between precipitation (soil moisture, Figure S1) and dust emission in Region D with *r* of -0.69 (-0.67).

Similar seasonality is also reported by Cowie et al. (2014), who suggested that the strongest dust season in winter in central Sahel is driven by strong harmattan winds and frequent Low level Jet breakdown, and the second peak in summer in west Sahel could be explained by the summer monsoon combined with the Sahara Heat Low. The study also suggested the dominance of strong wind frequency in the seasonal variation of the emission frequencies. Fiedler et al. (2013) also found a maximum of emission flux over the Bodélé Depression in winter and the highest emission flux in spring in west Sahara. The study suggested that near-surface peak winds associated with Nocturnal Low-Level Jets is a driver of mineral dust emissions. Negative correlation between dust emissions and soil moisture has also been revealed by Yu et al. (2017) and Pierre et al. (2012), as the decreased vegetation growth in response to dry soil would result in enhanced dust emissions.

It is also worth noting that the interannual variation in dust emission is much larger during the wet season (0.96 ± 0.25 Pg yr^{-1}, Table 3) than on an annual basis (0.73 ± 0.12 Pg yr^{-1}). Moreover, while the annual emissions gradually decrease from 2013 to 2017, the emissions during the wet season peak in 2015. The obviously different behavior between the annual emissions and emissions during the wet season suggests that predictions of future impact of African dust emissions over the Amazon Basin in response to climate change should focus on the wet season rather than the annual average, as the former is more related to the export of African dust towards the Amazon Basin.

4.2 Transatlantic transport of African dust

The amount of African dust reaching the Amazon Basin depends not only on the dust emission fluxes, but also the transport path. Associated with the annual oscillation of ITCZ, the outflow of African dust moves slightly southwest toward South America in boreal winter and spring, and moves west towards the Caribbean in boreal summer and fall (Moran-Zuloaga et al., 2018; Ben-Ami et al., 2012). Therefore, although higher dust load over the coastal region of North Africa is found in summer (> 500 mg m^{-2}), dust reaching the Amazon Basin is less than 10 mg m^{-2}. In contrast, dust load over the Amazon Basin could reach up to 50 mg m^{-2} in spring and winter.

In addition to the transport path, the changes in dust column burden along the transport towards the Amazon Basin are also sensitive to its removal rate, namely the lifetime against deposition over the Atlantic. Assuming first-order removal of dust aerosols, we further derived seasonal e-folding lifetime (hereinafter referred to as lifetime, τ) of simulated dust during 2013 − 2017, based on the logarithm of the dust column burden against travel time over the AOaTP (Figure 7) using Equation 1:

$$\tau = \frac{L}{v \times slope} \quad (1)$$

where L is the distance of 1-degree longitude averaged over 5° S − 25° N in unit of m $degree^{-1}$; v is the wind speed in unit of m s^{-1}; and *slope* is the gradient of the linear trend line based on the logarithm of dust burden against the distance in degree between 20 ºW and 50 ºW.

Estimated dust lifetime is the shortest (1.4 ± 0.098 d) in winter, followed by fall and

spring (1.9 ± 0.33 d and 2.3 ± 0.31 d, respectively), while the lifetime in summer is the longest (4.2 ± 0.68 d). The interannual variability of the lifetime is small in winter with relative standard deviation (RSD) of 7.0%, but relatively large in fall with RSD of 17%. The short lifetime in winter is generally associated with high deposition flux (including both dry and wet deposition). As shown in Figure 8, the largest dust deposition flux (> 1000 ng m^{-2} s^{-1}) is found over the source regions in northern Africa, especially in spring and winter, and is mainly due to dry deposition (accounting for more than 80%). As a result, 48% – 64% of total emission in northern Africa is deposited within the source region (Table S2). The deposition flux over the AOaTP, also shows strong seasonality, with a maximum of ~530 ng m^{-2} s^{-1} in winter and a minimum of ~180 ng m^{-2} s^{-1} in fall, and is mainly driven by wet deposition (accounting for 76% on average). The deposition over the AOaTP accounts for 20% of total emission in northern Africa in winter, in contrast to 7.7% in spring, consistent with the relatively shorter lifetime in winter discussed above.

The seasonality in the deposition fluxes and the consequent dust lifetime depends not only on precipitation but also the vertical pathways of dust transport across the Atlantic. Dust aerosols aloft at higher altitude reach further west and have relatively longer lifetime. Significant differences in dust vertical distributions along the transport pathways have been revealed from the CALIOP measurements, which show that more dust is transported above 2km in summer while the dust layer is the shallowest in winter (Liu et al., 2012).

4.3 The influence of African dust over the Amazon Basin

4.3.1 Surface aerosol concentrations

Figure 9 shows the time series of observed and simulated aerosol mass concentrations at ATTO in January − June for the period of 2014 − 2016. Observed mean concentration in wet season is 9.3 ± 7.6 μg m^{-3}, of which 83% is from coarse aerosol (7.7 μg m^{-3}), while simulated concentration is 11 ± 6.7 μg m^{-3}, with dust contribution of 65% (7.2 μg m^{-3}). The slight model bias could be to some extent explained by the difference in background concentrations (1.9 and 5.1 μg m^{-3} for the observation and model data, respectively). Most of observed peaks are found in February – March of 2014 and 2016,

and in February − April of 2015. The high correlation (r of 0.52 − 0.71) between observed coarse aerosols and simulated dust concentrations suggests that observed strong variation in coarse aerosols is mainly driven by the influence of dust. Rizzolo et al. (2017) conducted aerosol measurements at ATTO from 19 March to 24 April 2015. The study showed the arrival of African dust between 3 and 6 April when the highest concentrations of PM_{10}, soluble Fe (III) and Fe (II) were recorded at ATTO. The peak value of 23 μg m^{-3} for PM_{10} was observed on 5 April. This dust event is well reproduced in this study with the peak value of 28 μg m^{-3} for PM_{10} on the same day and the dust contribution to PM_{10} reaching above 70%. The co-occurrence of elevated sea salt concentration (reaching 2.5 μg m^{-3}) during this event is also found in this study, consistent with previous studies which show mixed transport of African dust and marine aerosol to the basin (Wang et al., 2016; Ben-Ami et al., 2010; Rizzolo et al., 2017; Adachi et al., 2020).

The dust peaks are generally associated with large dust emission and/or efficient trans-Atlantic transport (e.g. relatively longer lifetime). For example, the relatively higher dust concentrations in the wet season of 2015 (except for February) are generally associated with higher emissions (1.2 − 1.5 Pg yr^{-1}) compared with the year of 2014 and 2016 (0.68 – 1.0 Pg yr^{-1}, see Table S3). On the other hand, although emissions in February 2016 (0.95 Pg yr^{-1}) is slightly lower than those in February 2014 (1.2 Pg yr^{-1}), the relatively longer lifetime (1.7 d vs. 1.5 d) may help explain the high dust concentrations during that period. It should be noted that the lifetime estimated here represents the export efficiency averaged over a relatively large domain and a long-time scale (e.g. one month). Besides, the influence of African dust on the ATTO site is also subject to the variations of transport paths and precipitation fields.

Over the whole Amazon Basin, simulated mean surface dust concentrations in the wet season of 2013 − 2017 are 5.7 ± 1.3 μg m^{-3}, with a maximum of 7.9 μg m^{-3} in 2015 driven mainly by the relatively high dust emission flux. The maxima of surface dust concentrations are found in the northeast corner of rainforest (over 15 μg m^{-3}) with a clearly decreasing trend towards southwestern direction (Figure 10). The dust contribution to surface aerosol concentrations averaged over the whole basin is 40% ±

4.5%, again with the maximum of 48% found in 2015. The location with the largest dust contributions (up to 70% in the north corner) slightly shifted inland compared to the spatial distribution of dust concentration. This could be explained by relatively higher influence of sea salt aerosols along the coast (around 30-50% near the coast of South America). Although the emission fluxes of both sea salt and dust are largely determined by surface winds, the interannual variability of dust concentrations is larger than sea salt over the Amazon Basin (20% vs. 10%) as the former is also sensitive to the export efficiency across the Atlantic Ocean as discussed above. Figure 10c also shows the frequency of dust events over the Amazon Basin, estimated as the number of days when daily surface dust concentrations reaching the threshold of 9 μg m^{-3} (Moran-Zuloaga et al., 2018) divided by the total number of days in the wet season of 2013 − 2017. Dust frequency averaged over the whole region is around 18% ± 4.6% and decreases from 50 − 60% at the northeast coast to < 1% in southern inland. The frequency of dust events at ATTO site is around 32%, close to the median of the range. The interannual variation of the frequency (represented by RSD), however, has an opposite trend, gradually increasing from 10% at the northeast coast to over 100% in southern inland (36% at ATTO). During dust events, the dust mass concentration at ATTO reaches 16 ± 2.9 μg m^{-3} (three times as high as that over the whole wet season), accounting for around 75% ± 5.3% of total aerosol (Figure 10d). Similarly, under the influence of the long-range transport of Saharan dust plumes, Moran-Zuloaga et al. (2018) observed mass concentrations 14 ± 12 μg m^{-3} for coarse aerosol at the same site, accounting for 93% of total observed aerosol.

4.3.2 AOD

The contribution of DOD to AOD at 550 nm over most areas of the Amazon Basin (Figure 11) is in the range of 10 − 50% (23% ± 4.4% on average) during the wet season of 2013 − 2017, with maxima in the northern Amazon Basin. The dust contribution to total AOD is relatively smaller than that to surface aerosol concentrations, mainly because of the relatively lower MEE of dust aerosols

compared to other aerosols. There also exists large difference in DOD between the whole wet season and dust events: 0.021 ± 0.0055 vs. 0.055 ± 0.0076 averaged over the Amazon Basin. A maximum of 0.31 on a daily basis is found on 1 Mar 2016 at the northeast corner (55° W, 4° N) of the Amazon Basin during the study period. During dust events, dust aerosols dominate AOD (40% − 60%) over most regions of the Amazon Basin. At ATTO site, DOD is 0.034 ± 0.0088 and 0.063 ± 0.0087, accounting for 37% and 53% of AOD over the whole wet season and dust events, respectively. The largest dust contribution (up to 81%) with DOD of 0.18 at ATTO site is found on 24 Jan 2015. Consistent with our results, previous studies by Baars et al. (2011) and Baars et al. (2012) reported DOD (532 nm) of up to 0.18 and AOD of ~0.14 when affected by strong influence of Saharan dust at a similar Amazon site (60° 2.3′ W, 2° 35.9′ S).

4.3.3 Dust deposition and related nutrient input

The spatial distribution of dust deposition over the Amazon Basin is also shown in Figure 8. The mean dust deposition flux in wet season is 2.0 ± 0.35 g m^{-2} yr^{-1}, much higher than in dry seasons (August to November, 0.35 ± 0.16 g m^{-2} yr^{-1}). The maximum (2.6 g m^{-2} yr^{-1}) is found in the year 2015 due to relatively large dust emission and efficient trans-Atlantic transport. With emission of 0.96 ± 0.25 Pg yr^{-1} in wet season (0.73 ± 0.12 Pg yr^{-1} on annual average), only 1.9% (1.4%) of African dust is deposited into the Amazon Basin (dominated by wet deposition) while relatively large part is deposited over the AOaTP (13% in the wet season and 14% on annual average) and northern Africa (49% in the wet season).

Assuming mass fractions of 4.4%, 0.082%, and 1.8% for iron, phosphorus, and magnesium respectively in the African dust (Bristow et al., 2010; Chiemeka et al., 2007), we derive deposition fluxes of 88 ± 15 mg m^{-2} yr^{-1}, 1.6 ± 0.29 mg m^{-2} yr^{-1} and 36 ± 6.3 mg m^{-2} yr^{-1} for iron, phosphorus and magnesium respectively into the Amazon rainforest during the wet season and 52 ± 8.7, 0.97 ± 0.16 and 21 ± 3.6 mg m^{-2} yr^{-1} on annual average (Figure 12). It should be noted that there exits large spatial

variation of nutrient input into the Amazon Basin associated with the patterns of dust burden and dust deposition flux. The deposition flux decreases from over 70 mg m^{-2} yr^{-1} at northeast coast to less than 7 mg m^{-2} yr^{-1} in inland for magnesium and decreases from > 9 mg m^{-2} yr^{-1} at northeast coast to less than 1 mg m^{-2} yr^{-1} in southwestern Basin for phosphorus during the wet season. Similarly, the deposition flux of iron during the wet season decreases from over 500 mg m^{-2} yr^{-1} at northeast coast to less than 15 mg m^{-2} yr^{-1} in the southwest and is above 50 mg m^{-2} yr^{-1} in most of the Amazon Basin. It seems that the nutrient input from Africa dust may play a significant role in the northeastern part of the Amazon Basin, not in the southwest. Table 4 summarized the estimates of dust and associated phosphorus deposition into the Amazon Basin from previous studies. The estimated fluxes of dust and associated phosphorus deposition are in the range of 0.81 – 19 g m^{-2} yr^{-1} and 0.48 – 16 mg m^{-2} yr^{-1}. The large range is mainly driven by the high values (19 g m^{-2} yr^{-1} and 16 mg m^{-2} yr^{-1} for dust and associated phosphorus, respectively) from the study of Swap et al. (1992). Based on observations during storm events and dust climatology, the study estimated dust importation into the northeastern basin, which is most subject to the intrusion of African dust. Besides the discrepancy in defined regions, the wide range could also be partly explained by the application of different methods and associated intrinsic uncertainties as mentioned in the Introduction. For instance, the estimates from Swap et al. (1992) are mainly based on 1-month field measurements at three sites located in the northeastern basin. Assumption about air exchange rate across the coast to the basin, duration of dust storms as well as dust concentrations contained in the dust plumes had to been made to extrapolate the dust deposition into the Amazon Basin. Similarly, bias could also arise from insufficient observations available to constrain models or satellite retrievals. Additional uncertainty may also stem from the assumption about the P mass fraction, ranging from 0.07% to 0.108%. Our results are similar to the finding of Prospero et al. (2020), which has also been constrained by the observation at Cayenne.

According to Salati and Vose (1984), the total amount of phosphorous and magnesium

590 is 21.6 g m^{-2} and 29.8 g m^{-2}, respectively, in the ecosystem of the Amazon Basin (14.7
591 and 2.3 g m^{-2} respectively in the soil). On the other hand, Vitousek and Sanford
592 (1986) reported a loss of 0.8 − 4 mg m^{-2} yr^{-1} for phosphorus and 810 mg m^{-2} yr^{-1} for
593 magnesium in Brazilian ecosystem to surface waters. Estimated nutrient input from
594 African dust in our study accounts for 0.011% and 1.6% of total phosphorous and
595 magnesium in the soil over the Amazon Basin during the wet season (0.0066% and
596 0.91% on annual average), and could almost compensate the hydrologic losses of
597 phosphorous in Brazilian forest ecosystem. Similarly, Abouchami et al. (2013)
598 pointed out that most of the Amazonian rainforest is a system with an internal
599 recycling of nutrients. But the extra influx of nutrients from African dust might
600 account for a significant portion of the net ouflux, i.e. dissolved discharge of nutrients
601 into rivers. Keep in mind that the estimates of nutrients influx are subject to the
602 uncertainties in the estimates of dust flux as well as the mass fractions of nutrients
603 containted in the dust. In addition, marine aerosols and biomassburning aerosols
604 mixed with the LRT of African dust may also play a role for certain essential nutrients
605 (Prospero et al., 2020; Abouchami et al., 2013). More observations including the mass
606 fraction of nutrient in dust aerosols and the deposition fluxes of those elements in the
607 Amazon Basin are necessarily required in the future work to better evaluate the
608 nutrient input associated with the African dust intrusion.
609
610 **5 Conclusion**
611 In this study, we use the GEOS-Chem model with optimized particle mass size
612 distribution (PMSD) of dust aerosols to investigate the influence of the export of
613 African dust towards the Amazon Basin during 2013 – 2017. The model performance
614 is constrained by multiple datasets obtained from AERONET, MODIS, as well as
615 Cayenne and ATTO sites in the Amazon Basin. The optimized PMSD in this study
616 well captures observed AOD regarding both the mean value as well as the decline rate
617 of the logarithm of AOD over the Atlantic Ocean along the transport path (AOaTP),
618 while the other two PMSD schemes tend to overestimate the decline rate by 11% and

underestimate the mean value by up to ~40%.

Simulated dust emission from northern Africa is 0.73 ± 0.12 Pg yr^{-1}, accounting for more than 70% of global dust emission. There exists a strong seasonality in dust emission with peaks in spring or winter, which varies with source regions. The correlation analysis suggests high surface wind speeds and low soil moisture as a major driver for dust emissions. In addition to the transport path associated with the oscillation of ITCZ, the export efficiency of African dust towards the Amazon basin is sensitive to the removal of dust aerosol along the trans-Atlantic transport, which depends on both assumed PMSD of dust aerosols in the model and meteorological fields (i.e. precipitation and vertical transport path). The study further estimates the e-folding lifetime of dust aerosols along the trans-Atlantic transport based on the logarithm of the dust column burden against travel time over the AOaTP. The shortest lifetime (1.4 d) is found for winter associated with high deposition flux, while the highest dust burden over the AOaTP is found in summer mainly associated with its longer lifetime (4.2 d).

Simulated surface dust concentration averaged over the whole Amazon Basin is 5.7 ± 1.3 μg m^{-3} during the wet season of 2013 – 2017, contributing 40% ± 4.5% to total surface aerosols. Observed dust peaks at the ATTO site are generally associated with large dust emission and/or efficient trans-Atlantic transport. The frequency of dust events is 18% ± 4.6% averaged over the Amazon Basin and up to 50% − 60% at the northeast coast. During the dust events, DOD is around 0.055±0.0076 and dominate total AOD over most of the Amazon Basin. Associated with the deposition of African dust, the study estimated annual inputs of 52 ± 8.7, 0.97 ± 0.16 and 21 ± 3.6 mg m^{-2} yr^{-1} for iron, phosphorus and magnesium into the Amazon rainforest, which may well compensate the hydrologic losses of nutrients in the forest ecosystem.

Acknowledgements.

This work is supported by the National Natural Science Foundation of China (41907182, 41877303, 91644218), the National key R&D Program of China (2018YFC0213901), the

Fundamental Research Funds for the Central Universities (21621105), the Guangdong Innovative and Entrepreneurial Research Team Program (Research team on atmospheric environmental roles and effects of carbonaceous species: 2016ZT06N263), and Special Fund Project for Science and Technology Innovation Strategy of Guangdong Province (2019B121205004). We acknowledge the support by the Instituto Nacional de Pesquisas da Amazônia (INPA). We would like to thank all people involved in the technical, logistical, and scientific support within the ATTO project.

Financial support. This work is supported by the National Natural Science Foundation of China (41907182, 41877303, 91644218), the National key R&D Program of China (2018YFC0213901), the Fundamental Research Funds for the Central Universities (21621105), the Guangdong Innovative and Entrepreneurial Research Team Program (Research team on atmospheric environmental roles and effects of carbonaceous species: 2016ZT06N263), and Special Fund Project for Science and Technology Innovation Strategy of Guangdong Province (2019B121205004). For the operation of the ATTO site, we acknowledge the support by the Max Planck Society (MPG), the German Federal Ministry of Education and Research (BMBF contracts 01LB1001A, 01LK1602B, and 01LK2101B) and the Brazilian Ministério da Ciência, Tecnologia e Inovação (MCTI/FINEP contract 01.11.01248.00), the Amazon State University (UEA), FAPEAM, LBA/INPA, FAPESP - Fundação de Amparo à Pesquisa do Estado de São Paulo, grant number 2017/17047-0, and SDS/CEUC/RDS-Uatumã. XW acknowledges the financial support of China Scholarship Council (CSC). MP acknowledges the financial support by the Max Planck Graduate Center with the Johannes-Gutenberg University, Mainz.

Competing interests.

Hang Su and Yafang Cheng are members of the editorial board of Atmospheric Chemistry and Physics.

Data availability.

OPS data used in this study could be found at https://www.attodata.org/. Other datasets are available upon request.

References

Abouchami, W., Näthe, K., Kumar, A., Galer, S. J. G., Jochum, K. P., Williams, E., Horbe, A. M. C., Rosa, J. W. C., Balsam, W., Adams, D., Mezger, K., and Andreae, M. O.: Geochemical and isotopic characterization of the Bodélé Depression dust source and implications for transatlantic dust transport to the Amazon Basin, Earth Planet. Sc. Lett., 380, 112-123, https://doi.org/10.1016/j.epsl.2013.08.028, 2013.

Adachi, K., Oshima, N., Gong, Z., de Sá, S., Bateman, A. P., Martin, S. T., de Brito, J. F., Artaxo, P., Cirino, G. G., Sedlacek Iii, A. J., and Buseck, P. R.: Mixing states of Amazon basin aerosol particles transported over long distances using transmission electron microscopy, Atmos. Chem. Phys., 20, 11923-11939, 10.5194/acp-20-11923-2020, 2020.

Alizadeh-Choobari, O., Sturman, A., and Zawar-Reza, P.: A global satellite view of the seasonal distribution of mineral dust and its correlation with atmospheric circulation, Dynam. Atmos. Oceans, 68, 20-34, https://doi.org/10.1016/j.dynatmoce.2014.07.002, 2014.

Andreae, M. O., Berresheim, H., Bingemer, H., Jacob, D. J., Lewis, B. L., Li, S.-M., and Talbot, R. W.: The atmospheric sulfur cycle over the Amazon Basin: 2. Wet season, J. Geophys. Res., 95, 16813-16824, https://doi.org/10.1029/JD095iD10p16813, 1990.

Andreae, M. O., Acevedo, O. C., Araùjo, A., Artaxo, P., Barbosa, C. G. G., Barbosa, H. M. J., Brito, J., Carbone, S., Chi, X., Cintra, B. B. L., da Silva, N. F., Dias, N. L., Dias-Júnior, C. Q., Ditas, F., Ditz, R., Godoi, A. F. L., Godoi, R. H. M., Heimann, M., Hoffmann, T., Kesselmeier, J., Könemann, T., Krüger, M. L., Lavric, J. V., Manzi, A. O., Lopes, A. P., Martins, D. L., Mikhailov, E. F., Moran-Zuloaga, D., Nelson, B. W., Nölscher, A. C., Santos Nogueira, D., Piedade, M. T. F., Pöhlker, C., Pöschl, U., Quesada, C. A., Rizzo, L. V., Ro, C. U., Ruckteschler, N., Sá, L. D. A., de Oliveira Sá, M., Sales, C. B., dos Santos, R. M. N., Saturno, J., Schöngart, J., Sörgel, M., de Souza, C. M., de Souza, R. A. F., Su, H., Targhetta, N., Tóta, J., Trebs, I., Trumbore, S., van Eijck, A., Walter, D., Wang, Z., Weber, B., Williams, J., Winderlich, J., Wittmann, F., Wolff, S., and Yáñez-Serrano, A. M.: The Amazon Tall Tower Observatory (ATTO): overview of pilot measurements on ecosystem ecology, meteorology, trace gases, and aerosols, Atmos. Chem. Phys., 15, 10723-10776, 10.5194/acp-15-10723-2015, 2015.

Ansmann, A., Baars, H., Tesche, M., Müller, D., Althausen, D., Engelmann, R., Pauliquevis, T., and Artaxo, P.: Dust and smoke transport from Africa to South America: Lidar profiling over Cape Verde and the Amazon rainforest, Geophys. Res. Lett., 36, https://doi.org/10.1029/2009GL037923, 2009.

Baars, H., Ansmann, A., Althausen, D., Engelmann, R., Artaxo, P., Pauliquevis, T., and Souza, R.: Further evidence for significant smoke transport from Africa to Amazonia, Geophys. Res. Lett., 38, https://doi.org/10.1029/2011GL049200, 2011.

Baars, H., Ansmann, A., Althausen, D., Engelmann, R., Heese, B., Müller, D., Artaxo, P., Paixao, M., Pauliquevis, T., and Souza, R.: Aerosol profiling with lidar in the Amazon

719 Basin during the wet and dry season, J. Geophys. Res., 117,
720 https://doi.org/10.1029/2012JD018338, 2012.
721 Bakker, N. L., Drake, N. A., and Bristow, C. S.: Evaluating the relative importance of
722 northern African mineral dust sources using remote sensing, Atmos. Chem. Phys., 19,
723 10525-10535, 10.5194/acp-19-10525-2019, 2019.
724 Barkley, A. E., Prospero, J. M., Mahowald, N., Hamilton, D. S., Popendorf, K. J., Oehlert, A.
725 M., Pourmand, A., Gatineau, A., Panechou-Pulcherie, K., Blackwelder, P., and Gaston,
726 C. J.: African biomass burning is a substantial source of phosphorus deposition to the
727 Amazon, Tropical Atlantic Ocean, and Southern Ocean, Proceedings of the National
728 Academy of Sciences, 116, 16216-16221, 10.1073/pnas.1906091116, 2019.
729 Ben-Ami, Y., Koren, I., Altaratz, O., Kostinski, A., and Lehahn, Y.: Discernible rhythm in the
730 spatio/temporal distributions of transatlantic dust, Atmos. Chem. Phys., 12, 2253-2262,
731 10.5194/acp-12-2253-2012, 2012.
732 Ben-Ami, Y., Koren, I., Rudich, Y., Artaxo, P., Martin, S. T., and Andreae, M. O.: Transport of
733 North African dust from the Bodélé depression to the Amazon Basin: a case study,
734 Atmos. Chem. Phys., 10, 7533-7544, 10.5194/acp-10-7533-2010, 2010.
735 Bristow, C. S., Hudson-Edwards, K. A., and Chappell, A.: Fertilizing the Amazon and
736 equatorial Atlantic with West African dust, Geophys. Res. Lett., 37,
737 https://doi.org/10.1029/2010GL043486, 2010.
738 Chen, Y., Kreidenweis, S. M., McInnes, L. M., Rogers, D. C., and DeMott, P. J.: Single
739 particle analyses of ice nucleating aerosols in the upper troposphere and lower
740 stratosphere, Geophys. Res. Lett., 25, 1391-1394, 10.1029/97gl03261, 1998.
741 Chiemeka, I. U., Oleka, M. O., and Chineke, T.: Determination of aerosol metal composition
742 and concentration during the 2001/2002 Harmattan season at Uturu, Nigeria, Global J.
743 Pure Appl. Sci., 13, 10.4314/gjpas.v13i3.16734, 2007.
744 Cowie, S. M., Knippertz, P., and Marsham, J. H.: A climatology of dust emission events from
745 northern Africa using long-term surface observations, Atmos. Chem. Phys., 14, 8579-
746 8597, 10.5194/acp-14-8579-2014, 2014.
747 Demott, P. J., Sassen, K., Poellot, M. R., Baumgardner, D., Rogers, D. C., Brooks, S. D.,
748 Prenni, A. J., and Kreidenweis, S. M.: African dust aerosols as atmospheric ice nuclei,
749 Geophys. Res. Lett., 30, https://doi.org/10.1029/2003GL017410, 2003.
750 Di Biagio, C., Formenti, P., Balkanski, Y., Caponi, L., Cazaunau, M., Pangui, E., Journet, E.,
751 Nowak, S., Andreae, M. O., Kandler, K., Saeed, T., Piketh, S., Seibert, D., Williams, E.,
752 and Doussin, J. F.: Complex refractive indices and single-scattering albedo of global dust
753 aerosols in the shortwave spectrum and relationship to size and iron content, Atmos.
754 Chem. Phys., 19, 15503-15531, 10.5194/acp-19-15503-2019, 2019.
755 Drury, E., Jacob, D. J., Spurr, R. J. D., Wang, J., Shinozuka, Y., Anderson, B. E., Clarke, A.
756 D., Dibb, J., McNaughton, C., and Weber, R.: Synthesis of satellite (MODIS), aircraft
757 (ICARTT), and surface (IMPROVE, EPA-AQS, AERONET) aerosol observations over
758 eastern North America to improve MODIS aerosol retrievals and constrain surface
759 aerosol concentrations and sources, J. Geophys. Res., 115,
760 https://doi.org/10.1029/2009JD012629, 2010.
761 Dubovik, O., Holben, B., Eck, T. F., Smirnov, A., Kaufman, Y. J., King, M. D., Tanré, D., and
762 Slutsker, I.: Variability of Absorption and Optical Properties of Key Aerosol Types

Observed in Worldwide Locations, J. Atmos. Sci., 59, 590-608, http://doi.org/10.1175/1520-0469(2002)059<0590:VOAAOP>2.0.CO;2, 2002.

Duncan Fairlie, T., Jacob, D. J., and Park, R. J.: The impact of transpacific transport of mineral dust in the United States, Atmos. Environ., 41, 1251-1266, https://doi.org/10.1016/j.atmosenv.2006.09.048, 2007.

Dusek, U., Frank, G. P., Hildebrandt, L., Curtius, J., Schneider, J., Walter, S., Chand, D., Drewnick, F., Hings, S., Jung, D., Borrmann, S., and Andreae, M. O.: Size Matters More Than Chemistry for Cloud-Nucleating Ability of Aerosol Particles, Science, 312, 1375-1378, doi:10.1126/science.1125261, 2006.

Enfield, D. B., Mestas-Nuñez, A. M., and Trimble, P. J.: The Atlantic Multidecadal Oscillation and its relation to rainfall and river flows in the continental U.S, Geophys. Res. Lett., 28, 2077-2080, https://doi.org/10.1029/2000GL012745, 2001.

Evan, A. T., Flamant, C., Gaetani, M., and Guichard, F.: The past, present and future of African dust, Nature, 531, 493-495, 10.1038/nature17149, 2016.

Formenti, P., Andreae, M. O., Lange, L., Roberts, G., Cafmeyer, J., Rajta, I., Maenhaut, W., Holben, B. N., Artaxo, P., and Lelieveld, J.: Saharan dust in Brazil and Suriname during the Large-Scale Biosphere-Atmosphere Experiment in Amazonia (LBA) - Cooperative LBA Regional Experiment (CLAIRE) in March 1998, J. Geophys. Res., 106, 14919-14934, 10.1029/2000JD900827, 2001.

Gläser, G., Wernli, H., Kerkweg, A., and Teubler, F.: The transatlantic dust transport from North Africa to the Americas—Its characteristics and source regions, Journal of Geophysical Research: Atmospheres, 120, 11,231-211,252, https://doi.org/10.1002/2015JD023792, 2015.

Herbert, R. J., Krom, M. D., Carslaw, K. S., Stockdale, A., Mortimer, R. J. G., Benning, L. G., Pringle, K., and Browse, J.: The Effect of Atmospheric Acid Processing on the Global Deposition of Bioavailable Phosphorus From Dust, Global Biogeochemical Cycles, 32, 1367-1385, https://doi.org/10.1029/2018GB005880, 2018.

Highwood, E. J., Haywood, J. M., Silverstone, M. D., Newman, S. M., and Taylor, J. P.: Radiative properties and direct effect of Saharan dust measured by the C-130 aircraft during Saharan Dust Experiment (SHADE): 2. Terrestrial spectrum, J. Geophys. Res., 108, https://doi.org/10.1029/2002JD002552, 2003.

Holanda, B. A., Pöhlker, M. L., Walter, D., Saturno, J., Sörgel, M., Ditas, J., Ditas, F., Schulz, C., Franco, M. A., Wang, Q., Donth, T., Artaxo, P., Barbosa, H. M. J., Borrmann, S., Braga, R., Brito, J., Cheng, Y., Dollner, M., Kaiser, J. W., Klimach, T., Knote, C., Krüger, O. O., Fütterer, D., Lavrič, J. V., Ma, N., Machado, L. A. T., Ming, J., Morais, F. G., Paulsen, H., Sauer, D., Schlager, H., Schneider, J., Su, H., Weinzierl, B., Walser, A., Wendisch, M., Ziereis, H., Zöger, M., Pöschl, U., Andreae, M. O., and Pöhlker, C.: Influx of African biomass burning aerosol during the Amazonian dry season through layered transatlantic transport of black carbon-rich smoke, Atmos. Chem. Phys., 20, 4757-4785, 10.5194/acp-20-4757-2020, 2020.

Huneeus, N., Schulz, M., Balkanski, Y., Griesfeller, J., Prospero, J., Kinne, S., Bauer, S., Boucher, O., Chin, M., Dentener, F., Diehl, T., Easter, R., Fillmore, D., Ghan, S., Ginoux, P., Grini, A., Horowitz, L., Koch, D., Krol, M. C., Landing, W., Liu, X., Mahowald, N., Miller, R., Morcrette, J. J., Myhre, G., Penner, J., Perlwitz, J., Stier, P.,

Takemura, T., and Zender, C. S.: Global dust model intercomparison in AeroCom phase I, Atmos. Chem. Phys., 11, 7781-7816, 10.5194/acp-11-7781-2011, 2011.
Jaeglé, L., Quinn, P. K., Bates, T. S., Alexander, B., and Lin, J. T.: Global distribution of sea salt aerosols: new constraints from in situ and remote sensing observations, Atmos. Chem. Phys., 11, 3137-3157, 10.5194/acp-11-3137-2011, 2011.
Jimenez, J. L., Canagaratna, M. R., Donahue, N. M., Prevot, A. S. H., Zhang, Q., Kroll, J. H., DeCarlo, P. F., Allan, J. D., Coe, H., Ng, N. L., Aiken, A. C., Docherty, K. S., Ulbrich, I. M., Grieshop, A. P., Robinson, A. L., Duplissy, J., Smith, J. D., Wilson, K. R., Lanz, V. A., Hueglin, C., Sun, Y. L., Tian, J., Laaksonen, A., Raatikainen, T., Rautiainen, J., Vaattovaara, P., Ehn, M., Kulmala, M., Tomlinson, J. M., Collins, D. R., Cubison, M. J., Dunlea, J., Huffman, J. A., Onasch, T. B., Alfarra, M. R., Williams, P. I., Bower, K., Kondo, Y., Schneider, J., Drewnick, F., Borrmann, S., Weimer, S., Demerjian, K., Salcedo, D., Cottrell, L., Griffin, R., Takami, A., Miyoshi, T., Hatakeyama, S., Shimono, A., Sun, J. Y., Zhang, Y. M., Dzepina, K., Kimmel, J. R., Sueper, D., Jayne, J. T., Herndon, S. C., Trimborn, A. M., Williams, L. R., Wood, E. C., Middlebrook, A. M., Kolb, C. E., Baltensperger, U., and Worsnop, D. R.: Evolution of Organic Aerosols in the Atmosphere, Science, 326, 5959, 1525-1529, doi:10.1126/science.1180353, 2009.
Kaufman, Y. J.: Dust transport and deposition observed from the Terra-Moderate Resolution Imaging Spectroradiometer (MODIS) spacecraft over the Atlantic Ocean, Journal of Geophysical Research, 110, 10.1029/2003jd004436, 2005
Kim, D., Chin, M., Remer, L. A., Diehl, T., Bian, H., Yu, H., Brown, M. E., and Stockwell, W. R.: Role of surface wind and vegetation cover in multi-decadal variations of dust emission in the Sahara and Sahel, Atmos. Environ., 148, 282-296, https://doi.org/10.1016/j.atmosenv.2016.10.051, 2017.
Kim, D., Chin, M., Yu, H., Diehl, T., Tan, Q., Kahn, R. A., Tsigaridis, K., Bauer, S. E., Takemura, T., Pozzoli, L., Bellouin, N., Schulz, M., Peyridieu, S., Chédin, A., and Koffi, B.: Sources, sinks, and transatlantic transport of North African dust aerosol: A multimodel analysis and comparison with remote sensing data, J. Geophys. Res., 119, 6259-6277, https://doi.org/10.1002/2013JD021099, 2014.
Knippertz, P., Deutscher, C., Kandler, K., Müller, T., Schulz, O., and Schütz, L.: Dust mobilization due to density currents in the Atlas region: Observations from the Saharan Mineral Dust Experiment 2006 field campaign, J. Geophys. Res., 112, https://doi.org/10.1029/2007JD008774, 2007.
Koepke, P., Hess, M., Schult, I., and Shettle, E. P.: Global aerosol data set, Max-Planck Institute for Meteorology, 44, 1997.
Kok, J. F.: A scaling theory for the size distribution of emitted dust aerosols suggests climate models underestimate the size of the global dust cycle, Proc Natl Acad Sci U S A, 108, 1016-1021, 10.1073/pnas.1014798108, 2011.
Kok, J. F., Adebiyi, A. A., Albani, S., Balkanski, Y., Checa-Garcia, R., Chin, M., Colarco, P. R., Hamilton, D. S., Huang, Y., Ito, A., Klose, M., Li, L., Mahowald, N. M., Miller, R. L., Obiso, V., Pérez García-Pando, C., Rocha-Lima, A., and Wan, J. S.: Contribution of the world's main dust source regions to the global cycle of desert dust, Atmos. Chem. Phys., 21, 8169-8193, 10.5194/acp-21-8169-2021, 2021.
Li, Y., Randerson, J. T., Mahowald, N. M., and Lawrence, P. J.: Deforestation Strengthens

Atmospheric Transport of Mineral Dust and Phosphorus from North Africa to the Amazon, Journal of Climate, 34, 6087-6096, 10.1175/jcli-d-20-0786.1, 2021.
Liu, D., Taylor, J. W., Crosier, J., Marsden, N., Bower, K. N., Lloyd, G., Ryder, C. L., Brooke, J. K., Cotton, R., Marenco, F., Blyth, A., Cui, Z., Estelles, V., Gallagher, M., Coe, H., and Choularton, T. W.: Aircraft and ground measurements of dust aerosols over the west African coast in summer 2015 during ICE-D and AER-D, Atmos. Chem. Phys., 18, 3817-3838, 10.5194/acp-18-3817-2018, 2018.
Liu, H., Jacob, D. J., Bey, I., and Yantosca, R. M.: Constraints from 210Pb and 7Be on wet deposition and transport in a global three-dimensional chemical tracer model driven by assimilated meteorological fields, J. Geophys. Res., 106, 12109-12128, https://doi.org/10.1029/2000JD900839, 2001.
Lucchesi, R.: File Specification for GEOS-5 FP, GMAO Office Note No.4 (Version 1.0), 63 pp., available at: http://gmao.gsfc.nasa.gov/pubs/office_notes, 2013.
Mahowald, N., Albani, S., Engelstaedter, S., Winckler, G., and Goman, M.: Model insight into glacial–interglacial paleodust records, Quaternary Sci. Rev., 30, 832-854, https://doi.org/10.1016/j.quascirev.2010.09.007, 2011a.
Mahowald, N., Albani, S., Kok, J. F., Engelstaeder, S., Scanza, R., Ward, D. S., and Flanner, M. G.: The size distribution of desert dust aerosols and its impact on the Earth system, Aeolian Res., 15, 53-71, https://doi.org/10.1016/j.aeolia.2013.09.002, 2014.
Mahowald, N. M., Artaxo, P., Baker, A. R., Jickells, T. D., Okin, G. S., Randerson, J. T., and Townsend, A. R.: Impacts of biomass burning emissions and land use change on Amazonian atmospheric phosphorus cycling and deposition, Global Biogeochemical Cycles, 19, https://doi.org/10.1029/2005GB002541, 2005.
Mahowald, N., Ward, D. S., Kloster, S., Flanner, M. G., Heald, C. L., Heavens, N. G., Hess, P. G., Lamarque, J.-F., and Chuang, P. Y.: Aerosol Impacts on Climate and Biogeochemistry, Annu. Rev. Env. Resour., 36, 45-74, 10.1146/annurev-environ-042009-094507, 2011b.
Mahowald, N. M. and Kiehl, L. M.: Mineral aerosol and cloud interactions, Geophys. Res. Lett., 30, https://doi.org/10.1029/2002GL016762, 2003.
Mahowald, N. M., Muhs, D. R., Levis, S., Rasch, P. J., Yoshioka, M., Zender, C. S., and Luo, C.: Change in atmospheric mineral aerosols in response to climate: Last glacial period, preindustrial, modern, and doubled carbon dioxide climates, J. Geophys. Res., 111, https://doi.org/10.1029/2005JD006653, 2006.
Martin, R. V., Jacob, D. J., Yantosca, R. M., Chin, M., and Ginoux, P.: Global and regional decreases in tropospheric oxidants from photochemical effects of aerosols, J. Geophys. Res. , 108, https://doi.org/10.1029/2002JD002622, 2003.
Martin, S. T., Andreae, M. O., Artaxo, P., Baumgardner, D., Chen, Q., Goldstein, A. H., Guenther, A., Heald, C. L., Mayol-Bracero, O. L., McMurry, P. H., Pauliquevis, T., Pöschl, U., Prather, K. A., Roberts, G. C., Saleska, S. R., Silva Dias, M. A., Spracklen, D. V., Swietlicki, E., and Trebs, I.: Sources and properties of Amazonian aerosol particles, Rev. Geophys., 48, https://doi.org/10.1029/2008RG000280, 2010a.
Martin, S. T., Andreae, M. O., Althausen, D., Artaxo, P., Baars, H., Borrmann, S., Chen, Q., Farmer, D. K., Guenther, A., Gunthe, S. S., Jimenez, J. L., Karl, T., Longo, K., Manzi, A., Müller, T., Pauliquevis, T., Petters, M. D., Prenni, A. J., Pöschl, U., Rizzo, L. V.,

Schneider, J., Smith, J. N., Swietlicki, E., Tota, J., Wang, J., Wiedensohler, A., and Zorn, S. R.: An overview of the Amazonian Aerosol Characterization Experiment 2008 (AMAZE-08), Atmos. Chem. Phys., 10, 11415-11438, 10.5194/acp-10-11415-2010, 2010b.

Middleton, N.: Variability and Trends in Dust Storm Frequency on Decadal Timescales: Climatic Drivers and Human Impacts, Geosciences, 9, 261, http://doi.org/10.3390/geosciences9060261, 2019.

Moran-Zuloaga, D., Ditas, F., Walter, D., Saturno, J., Brito, J., Carbone, S., Chi, X., Hrabě de Angelis, I., Baars, H., Godoi, R. H. M., Heese, B., Holanda, B. A., Lavrič, J. V., Martin, S. T., Ming, J., Pöhlker, M. L., Ruckteschler, N., Su, H., Wang, Y., Wang, Q., Wang, Z., Weber, B., Wolff, S., Artaxo, P., Pöschl, U., Andreae, M. O., and Pöhlker, C.: Long-term study on coarse mode aerosols in the Amazon rain forest with the frequent intrusion of Saharan dust plumes, Atmos. Chem. Phys., 18, 10055-10088, 10.5194/acp-18-10055-2018, 2018.

Niedermeier, N., Held, A., Müller, T., Heinold, B., Schepanski, K., Tegen, I., Kandler, K., Ebert, M., Weinbruch, S., Read, K., Lee, J., Fomba, K. W., Müller, K., Herrmann, H., and Wiedensohler, A.: Mass deposition fluxes of Saharan mineral dust to the tropical northeast Atlantic Ocean: an intercomparison of methods, Atmos. Chem. Phys., 14, 2245-2266, 10.5194/acp-14-2245-2014, 2014.

Pöhlker, C., Walter, D., Paulsen, H., Könemann, T., Rodríguez-Caballero, E., Moran-Zuloaga, D., Brito, J., Carbone, S., Degrendele, C., Després, V. R., Ditas, F., Holanda, B. A., Kaiser, J. W., Lammel, G., Lavrič, J. V., Ming, J., Pickersgill, D., Pöhlker, M. L., Praß, M., Löbs, N., Saturno, J., Sörgel, M., Wang, Q., Weber, B., Wolff, S., Artaxo, P., Pöschl, U., and Andreae, M. O.: Land cover and its transformation in the backward trajectory footprint region of the Amazon Tall Tower Observatory, Atmos. Chem. Phys., 19, 8425-8470, 10.5194/acp-19-8425-2019, 2019.

Pöhlker, M. L., Ditas, F., Saturno, J., Klimach, T., Hrabě de Angelis, I., Araùjo, A. C., Brito, J., Carbone, S., Cheng, Y., Chi, X., Ditz, R., Gunthe, S. S., Holanda, B. A., Kandler, K., Kesselmeier, J., Könemann, T., Krüger, O. O., Lavrič, J. V., Martin, S. T., Mikhailov, E., Moran-Zuloaga, D., Rizzo, L. V., Rose, D., Su, H., Thalman, R., Walter, D., Wang, J., Wolff, S., Barbosa, H. M. J., Artaxo, P., Andreae, M. O., Pöschl, U., and Pöhlker, C.: Long-term observations of cloud condensation nuclei over the Amazon rain forest – Part 2: Variability and characteristics of biomass burning, long-range transport, and pristine rain forest aerosols, Atmos. Chem. Phys., 18, 10289-10331, 10.5194/acp-18-10289-2018, 2018.

Pöschl, U., Martin, S. T., Sinha, B., Chen, Q., Gunthe, S. S., Huffman, J. A., Borrmann, S., Farmer, D. K., Garland, R. M., Helas, G., Jimenez, J. L., King, S. M., Manzi, A., Mikhailov, E., Pauliquevis, T., Petters, M. D., Prenni, A. J., Roldin, P., Rose, D., Schneider, J., Su, H., Zorn, S. R., Artaxo, P., and Andreae, M. O.: Rainforest Aerosols as Biogenic Nuclei of Clouds and Precipitation in the Amazon, Science, 329, 1513-1516, doi:10.1126/science.1191056, 2010.

Prass, M., Andreae, M. O., de Araùjo, A. C., Artaxo, P., Ditas, F., Elbert, W., Förster, J. D., Franco, M. A., Hrabe de Angelis, I., Kesselmeier, J., Klimach, T., Kremper, L. A., Thines, E., Walter, D., Weber, J., Weber, B., Fuchs, B. M., Pöschl, U., and Pöhlker, C.:

939 Bioaerosols in the Amazon rain forest: temporal variations and vertical profiles of
940 Eukarya, Bacteria, and Archaea, Biogeosciences, 18, 4873-4887, 10.5194/bg-18-4873-
941 2021, 2021.
942 Prospero, J. M., Glaccum, R. A., and Nees, R. T.: Atmospheric transport of soil dust from
943 Africa to South America, Nature, 289, 570-572, 10.1038/289570a0, 1981.
944 Prospero, J. M., Collard, F.-X., Molinié, J., and Jeannot, A.: Characterizing the annual cycle
945 of African dust transport to the Caribbean Basin and South America and its impact on the
946 environment and air quality, Global Biogeochem. Cy., 28, 757-773,
947 https://doi.org/10.1002/2013GB004802, 2014.
948 Prospero, J. M., Barkley, A. E., Gaston, C. J., Gatineau, A., Campos y Sansano, A., and
949 Panechou, K.: Characterizing and Quantifying African Dust Transport and Deposition to
950 South America: Implications for the Phosphorus Budget in the Amazon Basin, Global
951 Biogeochem. Cy., 34, e2020GB006536, https://doi.org/10.1029/2020GB006536, 2020.
952 Ridley, D. A., Heald, C. L., and Ford, B.: North African dust export and deposition: A satellite
953 and model perspective, J. Geophys. Res., 117, https://doi.org/10.1029/2011JD016794,
954 2012.
955 Ridley, D. A., Heald, C. L., and Prospero, J. M.: What controls the recent changes in African
956 mineral dust aerosol across the Atlantic?, Atmos. Chem. Phys., 14, 5735-5747,
957 10.5194/acp-14-5735-2014, 2014.
958 Rizzolo, J. A., Barbosa, C. G. G., Borillo, G. C., Godoi, A. F. L., Souza, R. A. F., Andreoli, R.
959 V., Manzi, A. O., Sá, M. O., Alves, E. G., Pöhlker, C., Angelis, I. H., Ditas, F., Saturno,
960 J., Moran-Zuloaga, D., Rizzo, L. V., Rosário, N. E., Pauliquevis, T., Santos, R. M. N.,
961 Yamamoto, C. I., Andreae, M. O., Artaxo, P., Taylor, P. E., and Godoi, R. H. M.: Soluble
962 iron nutrients in Saharan dust over the central Amazon rainforest, Atmos. Chem. Phys.,
963 17, 2673-2687, 10.5194/acp-17-2673-2017, 2017.
964 Roberts, A. and Knippertz, P.: Haboobs: Convectively generated dust storms in West Africa,
965 Weather, 67, 311 - 316, 2012.
966 Ryder, C. L., Highwood, E. J., Lai, T. M., Sodemann, H., and Marsham, J. H.: Impact of
967 atmospheric transport on the evolution of microphysical and optical properties of
968 Saharan dust, Geophys. Res. Lett., 40, 2433-2438, 10.1002/grl.50482, 2013a.
969 Ryder, C. L., Highwood, E. J., Rosenberg, P. D., Trembath, J., Brooke, J. K., Bart, M., Dean,
970 A., Crosier, J., Dorsey, J., Brindley, H., Banks, J., Marsham, J. H., McQuaid, J. B.,
971 Sodemann, H., and Washington, R.: Optical properties of Saharan dust aerosol and
972 contribution from the coarse mode as measured during the Fennec 2011 aircraft
973 campaign, Atmos. Chem. Phys., 13, 303-325, 10.5194/acp-13-303-2013, 2013b.
974 Ryder, C. L., Marenco, F., Brooke, J. K., Estelles, V., Cotton, R., Formenti, P., McQuaid, J. B.,
975 Price, H. C., Liu, D., Ausset, P., Rosenberg, P. D., Taylor, J. W., Choularton, T., Bower,
976 K., Coe, H., Gallagher, M., Crosier, J., Lloyd, G., Highwood, E. J., and Murray, B. J.:
977 Coarse-mode mineral dust size distributions, composition and optical properties from
978 AER-D aircraft measurements over the tropical eastern Atlantic, Atmos. Chem. Phys.,
979 18, 17225-17257, 10.5194/acp-18-17225-2018, 2018.
980 Salati, E. and Vose, P. B.: Amazon Basin: A System in Equilibrium, Science, 225, 129-138,
981 doi:10.1126/science.225.4658.129, 1984.
982 Shao, Y., Fink, A. H., and Klose, M.: Numerical simulation of a continental-scale Saharan

dust event, J. Geophys. Res., 115, https://doi.org/10.1029/2009JD012678, 2010.
Shao, Y., Klose, M., and Wyrwoll, K.-H.: Recent global dust trend and connections to climate forcing, J. Geophys. Res., 118, 11,107-111,118, https://doi.org/10.1002/jgrd.50836, 2013.
Sinyuk, A., Torres, O., and Dubovik, O.: Combined use of satellite and surface observations to infer the imaginary part of refractive index of Saharan dust, Geophys. Res. Lett., 30, https://doi.org/10.1029/2002GL016189, 2003.
SWAP, R., GARSTANG, M., GRECO, S., TALBOT, R., and KÅLLBERG, P.: Saharan dust in the Amazon Basin, Tellus B, 44, 133-149, https://doi.org/10.1034/j.1600-0889.1992.t01-1-00005.x, 1992.
Talbot, R. W., Andreae, M. O., Berresheim, H., Artaxo, P., Garstang, M., Harriss, R. C., Beecher, K. M., and Li, S. M.: Aerosol chemistry during the wet season in central Amazonia: The influence of long-range transport, J. Geophys. Res., 95, 16955-16969, https://doi.org/10.1029/JD095iD10p16955, 1990.
van der Does, M., Korte, L. F., Munday, C. I., Brummer, G. J. A., and Stuut, J. B. W.: Particle size traces modern Saharan dust transport and deposition across the equatorial North Atlantic, Atmos. Chem. Phys., 16, 13697-13710, 10.5194/acp-16-13697-2016, 2016.
Vitousek, P. M. and Sanford, R. L.: Nutrient Cycling in Moist Tropical Forest, Annual Review of Ecology and Systematics, 17, 137-167, http://www.jstor.org/stable/2096992.1986.
Wang, J., Christopher, S. A., Brechtel, F., Kim, J., Schmid, B., Redemann, J., Russell, P. B., Quinn, P., and Holben, B. N.: Geostationary satellite retrievals of aerosol optical thickness during ACE-Asia, J. Geophys. Res., 108, https://doi.org/10.1029/2003JD003580, 2003a.
Wang, J., Christopher, S. A., Reid, J. S., Maring, H., Savoie, D., Holben, B. N., Livingston, J. M., Russell, P. B., and Yang, S.-K.: GOES 8 retrieval of dust aerosol optical thickness over the Atlantic Ocean during PRIDE, J. Geophys. Res., 108, https://doi.org/10.1029/2002JD002494, 2003b.
Wang, Q., Gu, J., and Wang, X.: The impact of Sahara dust on air quality and public health in European countries, Atmospheric Environment, 241, 117771, https://doi.org/10.1016/j.atmosenv.2020.117771, 2020.
Wang, Q., Jacob, D. J., Fisher, J. A., Mao, J., Leibensperger, E. M., Carouge, C. C., Le Sager, P., Kondo, Y., Jimenez, J. L., Cubison, M. J., and Doherty, S. J.: Sources of carbonaceous aerosols and deposited black carbon in the Arctic in winter-spring: implications for radiative forcing, Atmos. Chem. Phys., 11, 12453-12473, 10.5194/acp-11-12453-2011, 2011.
Wang, Q., Saturno, J., Chi, X., Walter, D., Lavric, J. V., Moran-Zuloaga, D., Ditas, F., Pöhlker, C., Brito, J., Carbone, S., Artaxo, P., and Andreae, M. O.: Modeling investigation of light-absorbing aerosols in the Amazon Basin during the wet season, Atmos. Chem. Phys., 16, 14775-14794, 10.5194/acp-16-14775-2016, 2016.
Wang, W., Evan, A. T., Lavaysse, C., and Flamant, C.: The role the Saharan Heat Low plays in dust emission and transport during summertime in North Africa, Aeolian Res., 28, 1-12, https://doi.org/10.1016/j.aeolia.2017.07.001, 2017.
Wang, Y., Jacob, D. J., and Logan, J. A.: Global simulation of tropospheric O3-NO x - hydrocarbon chemistry: 1. Model formulation, J. Geophys. Res. , 103, 10713-10725,

https://doi.org/10.1029/98JD00158, 1998.
Wesely, M. L.: Parameterization of surface resistances to gaseous dry deposition in regional-scale numerical models, Atmos. Environ., 41, 52-63, https://doi.org/10.1016/j.atmosenv.2007.10.058, 2007.
White, B. R.: soil transport by winds on Mars, Journal of Geophysical Research: Solid Earth, 84, 4643-4651, https://doi.org/10.1029/JB084iB09p04643, 1979.
Wu, L., Li, X., Kim, H., Geng, H., Godoi, R. H. M., Barbosa, C. G. G., Godoi, A. F. L., Yamamoto, C. I., de Souza, R. A. F., Pöhlker, C., Andreae, M. O., and Ro, C. U.: Single-particle characterization of aerosols collected at a remote site in the Amazonian rainforest and an urban site in Manaus, Brazil, Atmos. Chem. Phys., 19, 1221-1240, 10.5194/acp-19-1221-2019, 2019.
Ysard, N., Jones, A. P., Demyk, K., Boutéraon, T., and Koehler, M.: The optical properties of dust: the effects of composition, size, and structure, A&A, 617, A124, 2018.
Yu, H., Chin, M., Bian, H., Yuan, T., Prospero, J. M., Omar, A. H., Remer, L. A., Winker, D. M., Yang, Y., Zhang, Y., and Zhang, Z.: Quantification of trans-Atlantic dust transport from seven-year (2007–2013) record of CALIPSO lidar measurements, Remote Sens. Environ., 159, 232-249, https://doi.org/10.1016/j.rse.2014.12.010, 2015a.
Yu, H., Chin, M., Yuan, T., Bian, H., Remer, L. A., Prospero, J. M., Omar, A., Winker, D., Yang, Y., Zhang, Y., Zhang, Z., and Zhao, C.: The fertilizing role of African dust in the Amazon rainforest: A first multiyear assessment based on data from Cloud-Aerosol Lidar and Infrared Pathfinder Satellite Observations, Geophys. Res. Lett., 42, 1984-1991, 10.1002/2015GL063040, 2015b.
Yu, Y., Kalashnikova, O. V., Garay, M. J., Lee, H., Notaro, M., Campbell, J. R., Marquis, J., Ginoux, P., and Okin, G. S.: Disproving the Bodélé Depression as the Primary Source of Dust Fertilizing the Amazon Rainforest, Geophysical Research Letters, 47, 2020.
Yu, H., Tan, Q., Chin, M., Remer, L. A., Kahn, R. A., Bian, H., Kim, D., Zhang, Z., Yuan, T., Omar, A. H., Winker, D. M., Levy, R. C., Kalashnikova, O., Crepeau, L., Capelle, V., and Chédin, A.: Estimates of African Dust Deposition Along the Trans-Atlantic Transit Using the Decadelong Record of Aerosol Measurements from CALIOP, MODIS, MISR, and IASI, J. Geophys. Res., 124, 7975-7996, https://doi.org/10.1029/2019JD030574, 2019.
Yuan, T., Yu, H., Chin, M., Remer, L. A., McGee, D., and Evan, A.: Anthropogenic Decline of African Dust: Insights From the Holocene Records and Beyond, Geophys. Res. Lett., 47, e2020GL089711, https://doi.org/10.1029/2020GL089711, 2020.
Zender, C. S., Bian, H., and Newman, D.: Mineral Dust Entrainment and Deposition (DEAD) model: Description and 1990s dust climatology, J. Geophys. Res., 108, https://doi.org/10.1029/2002JD002775, 2003.
Zhang, L., Gong, S., Padro, J., and Barrie, L.: A size-segregated particle dry deposition scheme for an atmospheric aerosol module, Atmos. Environ., 35, 549-560, https://doi.org/10.1016/S1352-2310(00)00326-5, 2001.
Zhang, L., Kok, J. F., Henze, D. K., Li, Q., and Zhao, C.: Improving simulations of fine dust surface concentrations over the western United States by optimizing the particle size distribution, Geophys. Res. Lett., 40, 3270-3275, 10.1002/grl.50591, 2013.

Table 1. Mass fractions (%) of dust emitted in each bin for different particle mass size distribution (PMSD) schemes tested in GEOS-Chem.

Scheme	bin 1				bin 2	bin 3	bin 4
	sub-bin 1	sub-bin 2	sub-bin 3	sub-bin 4			
	(0.1 – 0.18)[a]	(0.18 – 0.3)[a]	(0.3 – 0.6)[a]	(0.6 – 1.0)[a]	(1.0 – 1.8)[a]	(1.8 – 3.0)[a]	(3.0 – 6.0)[a]
	(3.1)[b]	(4.3)[b]	(2.7)[b]	(0.96)[b]	(0.45)[b]	(0.27)[b]	(0.16)[b]
V12	0.7	7.7 3.32	24.87	71.11	19.2	34.9	38.2
V12_C	6	12.2 12	24	58.00	25.3	32.2	30.2
V12_F	3.9	5.5 8.06	43	45.04	11.9	15.6	67

[a] size range in radius (μm) for each bin

[b] mass extinction efficiency (MEE) at wavelength of 550 nm in unit of m^2 g^{-1} for dust particles in each bin in the GEOS-Chem mod

Table 2. Summary of the observations used in this study, including the parameters, the spatio-temporal coverage, and the corresponding application in the model.

Datasets	Parameters	Locations	Periods (resolution)	Application
AERONET	AOD	northern Africa, the Atlantic Ocean	2013 – 2017 (daily)	Model AOD evaluation over northern Africa and the Atlantic Ocean
Fennec Campaign	PVSD[a]	northern Africa	2013 – 2017 (daily)	Model dust PMSD evaluation
	PMSD[b]	Over Mali and Algeria, Africa	17 – 28 June, 2011	Model dust PMSD evaluation
MODIS	AOD	northern Africa and the Atlantic Ocean	2013 – 2017 (daily)	Model AOD evaluation over northern Africa and the Atlantic Ocean
Cayenne	PM_{10}	52.3097° W, 4.9489° N (France)	January – April, 2014 (daily)	Model dust mass concentration evaluation at the coast of South America
ATTO	PNSD[c]	59.0056° W, 2.1459° S (Brazil)	January – April, 2014 – 2016 (5 min)	Model dust mass concentration evaluation at the central Amazon Basin

[a] particle volume size distribution; [b] particle mass size distribution; [c] particle number size distribution

Table 3. Annual and seasonal dust emissions (Pg yr^{-1}) in northern Africa (17.5° W – 40° E, 10° N – 35° N)[a].

Year	Spring	Summer	Fall	Winter	Annual (Wet season)
2013	1.2	0.77	0.48	1.0	0.88 (1.1)
2014	0.83	0.84	0.51	0.91	0.77 (0.89)
2015	1.2	0.46	0.33	1.1	0.77 (1.3)
2016	0.82	0.52	0.37	0.89	0.65 (0.86)
2017	0.68	0.38	0.47	0.70	0.56 (0.63)
Mean±std[b]	0.95±0.24	0.59±0.20	0.43±0.078	0.92±0.15	0.73±0.12 (0.96±0.25)

[a] Spring: March – May; Summer: June – August; Fall: September – November; Winter: January, February, and December; Wet season: January – April

[b] standard deviation

Table 4. Estimates of annual dust and associated phosphorus deposition into the Amazon Basin.

Methods	Dust deposition		P deposition		References
	total ($Tg\ a^{-1}$)	flux ($g\ m^{-2}\ a^{-1}$)	total ($Tg\ a^{-1}$)	flux ($mg\ m^{-2}\ a^{-1}$)	
CESM2	10 ± 2.1	n/a	0.0077±0.0016	n/a	Li et al. (2021)[a]
AeroCom Phase I	7.7	0.81	0.0063	0.66	Kok et al. (2021)[b]
MERRA-2	8.0	1.05	0.0062	0.9	Prospero et al. (2020)[a]
MERRA-2, CAM	n/a	n/a	0.011 – 0.033	1.1 – 3.5	Barkley et al. (2019)[a]
GLOMAP	32	1.8	0.019	1.1	Herbert et al. (2018)[a]
CALIOP	8− 48	0.8 − 5	0.006 – 0.037	0.7 – 3.9	Yu et al. (2015b)[a]
ECHAM5	30.3/11.4	n/a	0.025/0.0093	n/a	Gläser et al. (2015)[b]
GEOS-Chem	17± 5	n/a	0.014	n/a	Ridley et al. (2012)[b]
MATCH	n/a	n/a	n/a	0.48	Mahowald et al. (2005)[a]
MODIS	50	n/a	0.041	n/a	Kaufman (2005)[b]
Field measurement	13	19	0.011	16	Swap et al. (1992)[b]

GEOS-Chem	10 ± 1.7	1.2 ± 0.20	0.0085 ± 0.0014	0.97 ± 0.16	This study

Note. Table extracted in part from Prospero et al. (2020).

[a] The P mass fraction is 0.077% for Li et al. (2021) and Prospero et al. (2020), 0.108% for Barkley et al. (2019), 0.088% for Herbert et al. (2018), 0.078% for Yu et al. (2015b), and 0.07% for Mahowald et al. (2005).

[b] Assuming P mass fraction of 0.082% in dust, the same value as used in this study.

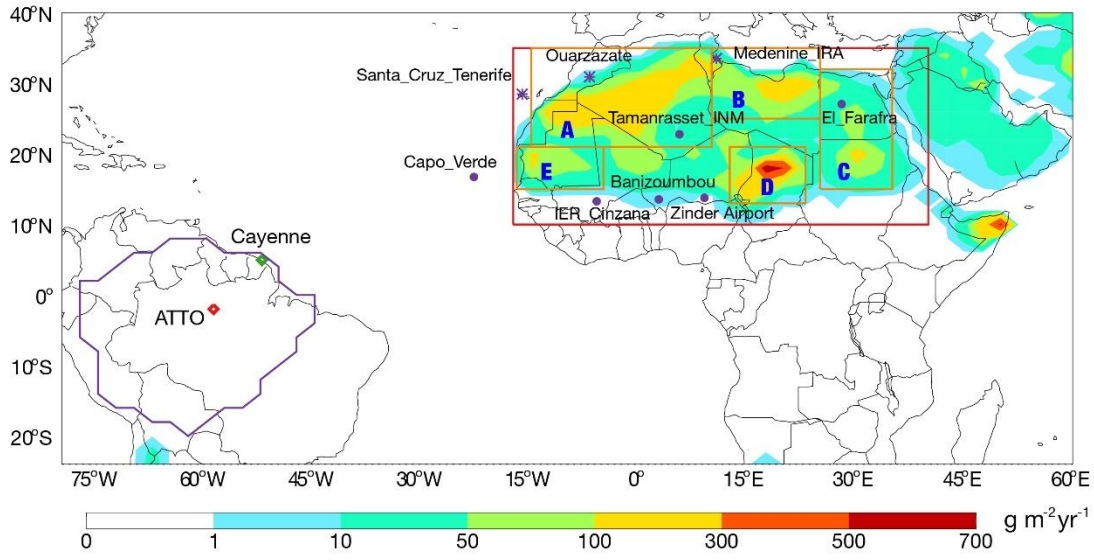

Figure 1. Simulated annual dust emissions in GEOS-Chem, averaged from 2013 to 2017. The location of AERONET sites used in Figure 2 are marked as purple symbols, of which circles represent the sites used in Figure 3. The region of the Amazon Basin is defined by purple lines. The location of Cayenne site in the northeast coast of South America and ATTO site in the central Amazon Basin are marked as green and red diamonds, respectively. The red rectangle illustrates the area of northern Africa (17.5° W – 40° E, 10° N – 35° N) and the orange rectangles shows the areas of five major source regions described in the text (A: 15° W – 10° E, 21° N – 35° N; B: 10° E – 25° E, 25° N – 35°N; C: 25° E – 35° E, 15° N – 32° N; D: 12.5° E – 23° E, 13° N – 21° N; E: 17° W – 5°W, 15° N – 21° N).

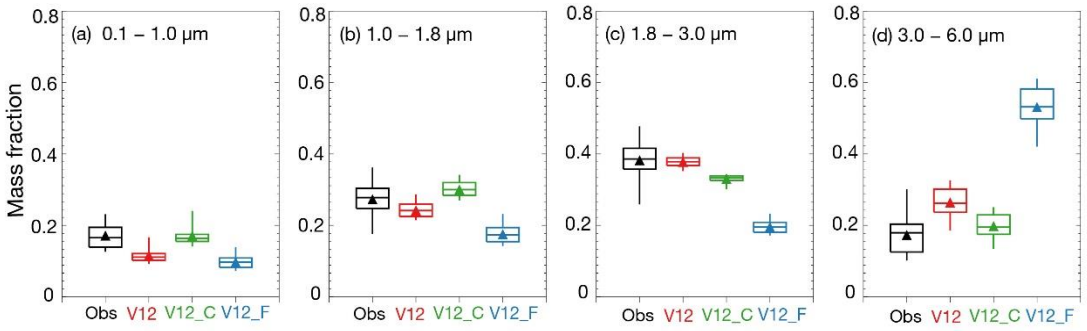

Figure 2. Boxplots of the mass fractions of column-integrated aerosols in the four size bins (in radius) retrieved from AERONET sites over Africa compared with model results based on different PMSD schemes. The triangles represent the mean values.

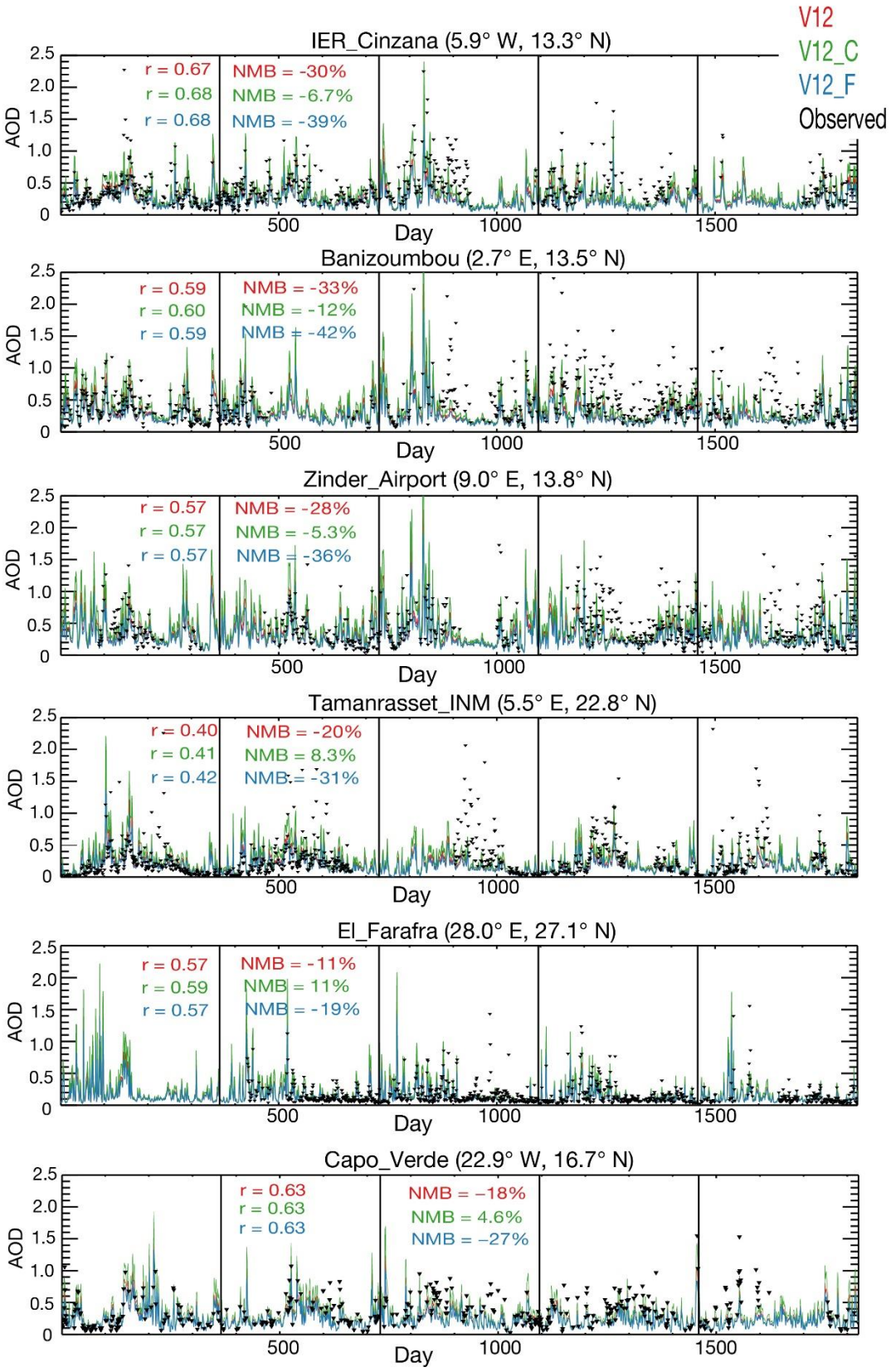

Figure 3. Time series of AERONET (black lines) and simulated daily AOD (at wavelength of 675 nm) during 2013 – 2017. Normalized mean bias (NMB) and correlation (*r*) statistics between the

AERONET and simulated data are shown as inset.

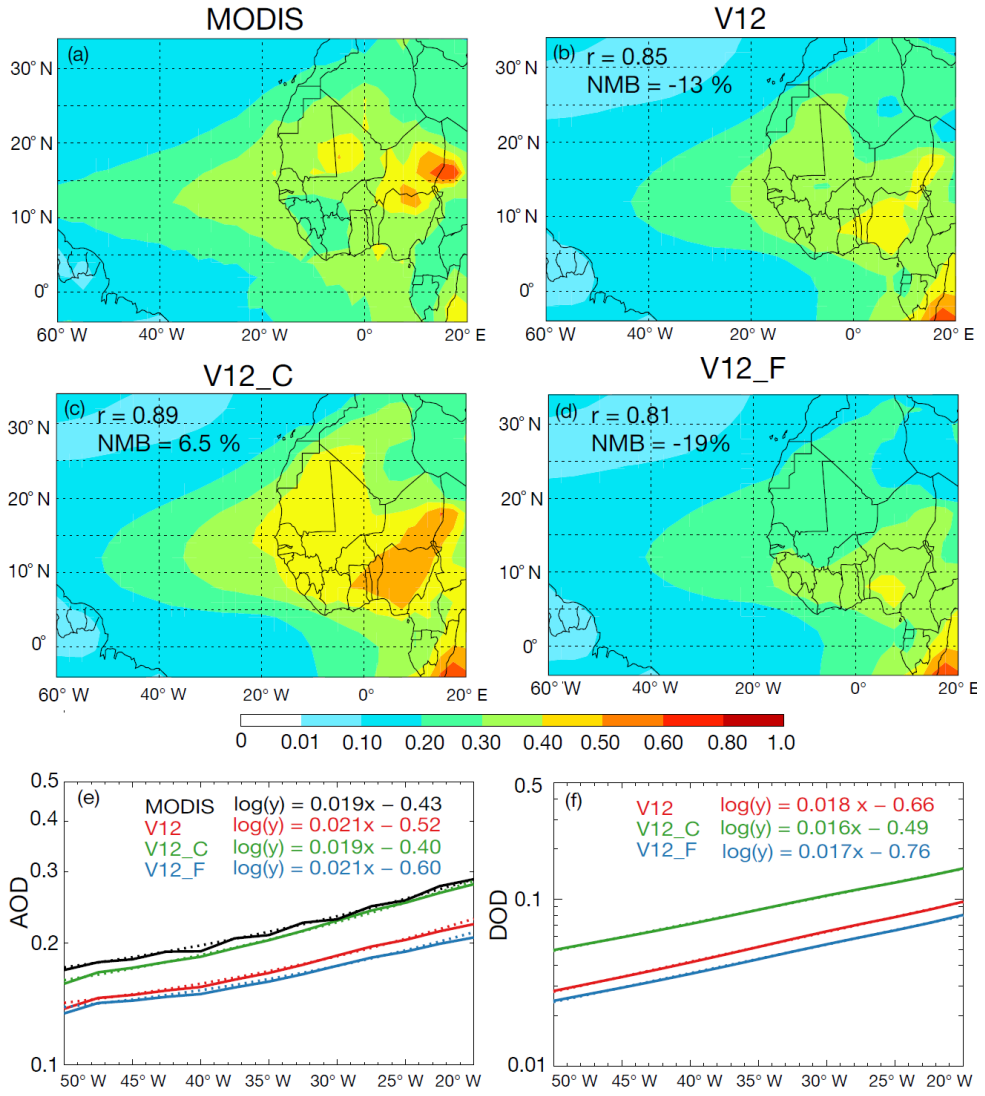

Figure 4. (a) – (d) Spatial distributions of observed and simulated AOD (at 550 nm) over the region of 60° W – 20° E and 10° N – 35° N averaged over 2013 – 2017. Normalized mean bias (NMB) and correlation coefficient (r) between the simulations and MODIS AOD are shown as inset. (e) MODIS (black) and simulated (color) AOD and (f) simulated dust optical depth (DOD) at 550 nm along the transect from 20° to 50° W, averaged over 5° S − 25° N for the period 2013 − 2017. The solid lines represent averaged data and the dashed lines are the logarithmic trend lines.

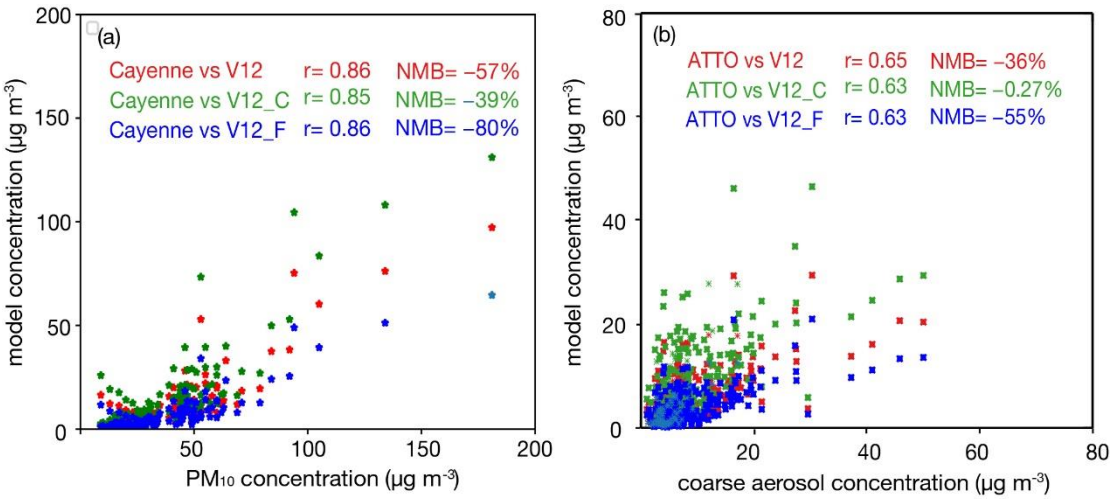

Figure 5. Scatter plots of (a) observed PM_{10} and simulated dust concentrations at Cayenne site during wet season of 2014 and (b) observed coarse aerosol ($PM_{1\text{-}10}$) and simulated dust concentrations at ATTO site during wet season of 2014-2016. Normalized mean bias (NMB) and correlation (*r*) statistics between the observation and simulation are shown as inset.

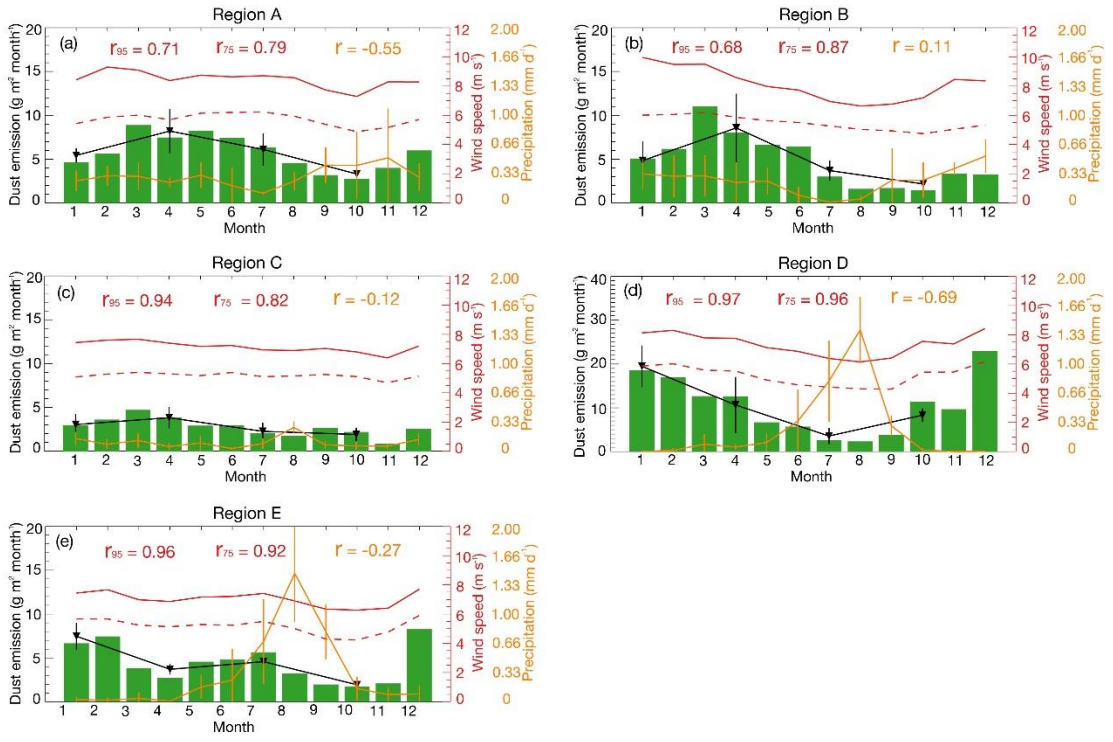

Figure 6. Monthly dust emission fluxes together with the 95th percentile hourly 10-m wind speeds (red solid lines), the 75th percentile hourly 10-m wind speeds (red dotted lines) and precipitation (yellow lines) over the five major source regions averaged from 2013 to 2017. Seasonal emission fluxes of dust are also shown as black lines. The correlation coefficients (r) between the dust emission fluxes and different meteorological variables are also shown in each panel.

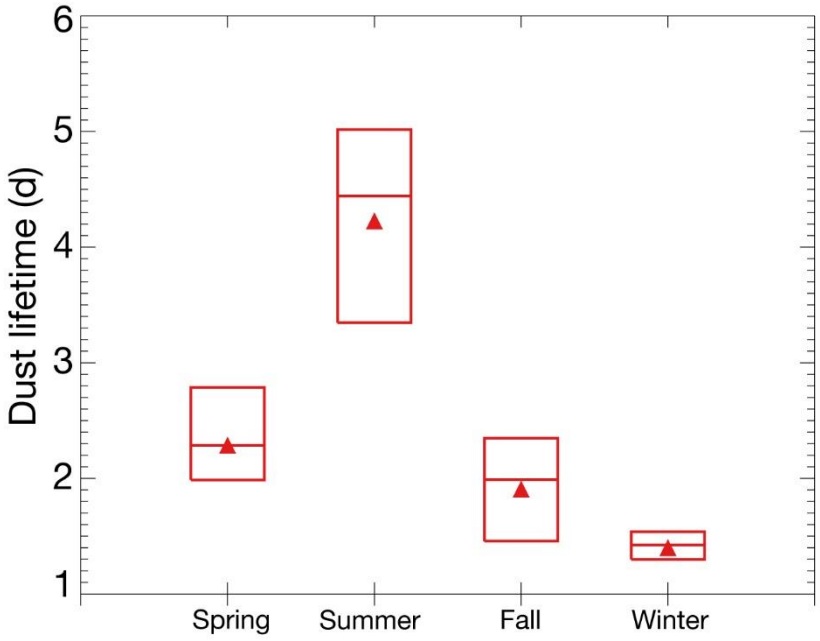

Figure 7. Seasonal e-folding lifetime derived from the logarithm of simulated dust column burden against travel time along the transect from 20° W to 50° W averaged over 5° S − 25° N during the period of 2013 – 2017. The triangles represent the mean values, and the bottom and top sides of the boxes represent the minimums and maximums.

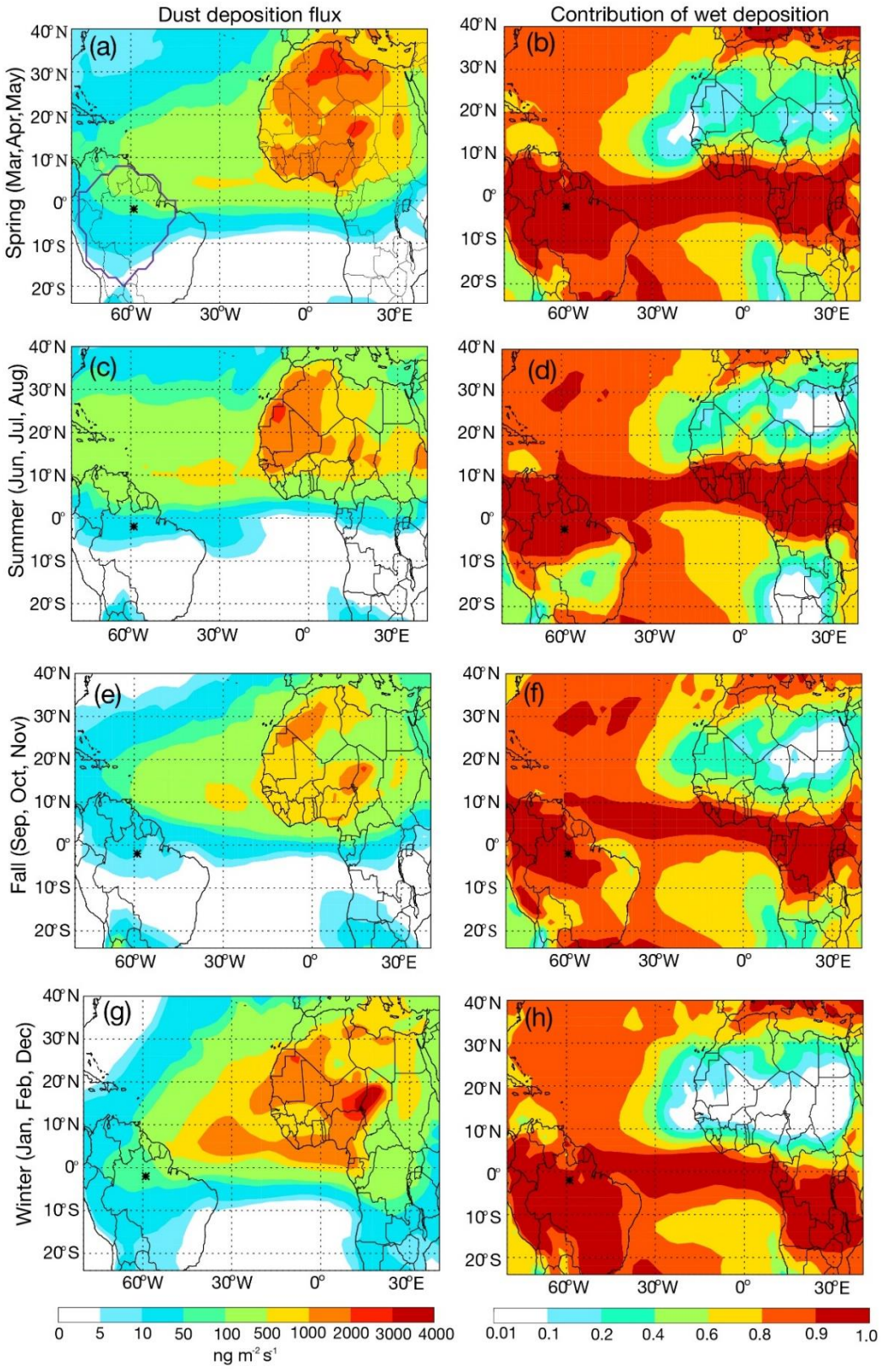

Figure 8. Simulated seasonal (left) dust deposition fluxes and (right) contribution of wet deposition during 2013-2017. The ATTO site is marked as asterisk. The region of the Amazon Basin is defined by purple lines in Figure 8a.

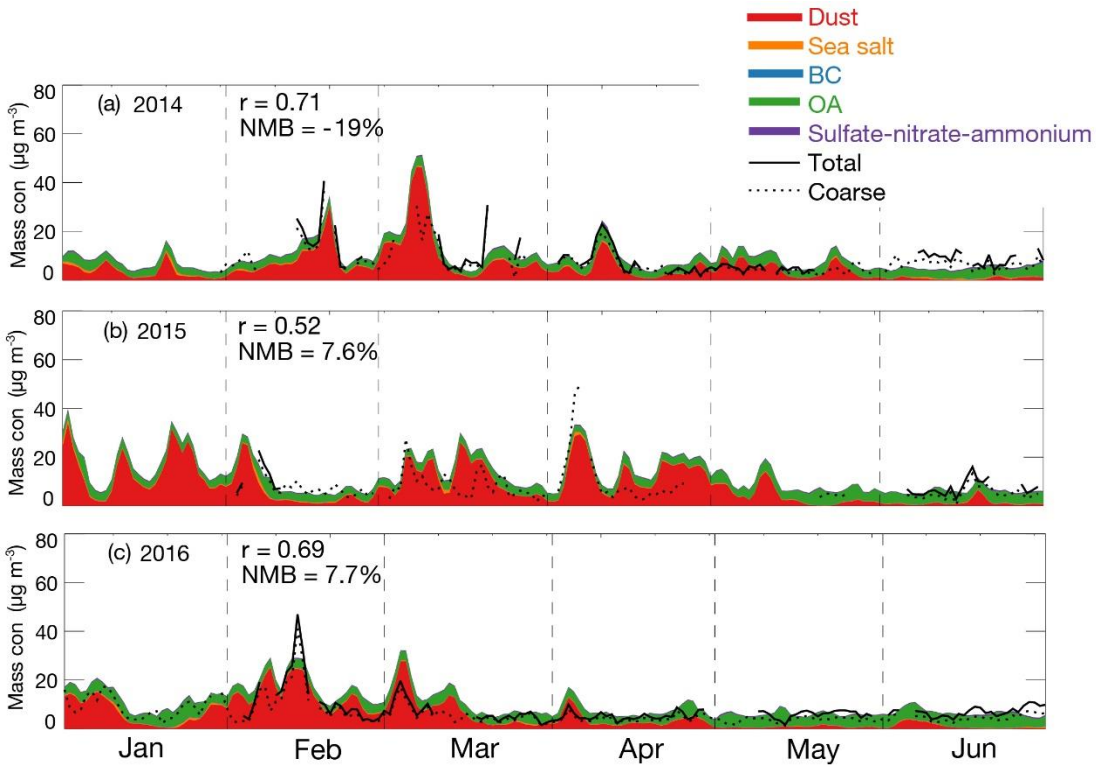

Figure 9. Time series of observed coarse and total aerosol mass concentrations and simulated aerosol species concentrations at the ATTO site from January to June in (a) 2014, (b) 2015, and (c) 2016. Model results are separated into different species shown as stacked areas. Normalized mean bias (NMB) and correlation coefficient (r) between the observed coarse aerosols and simulated dust concentrations are shown as inset.

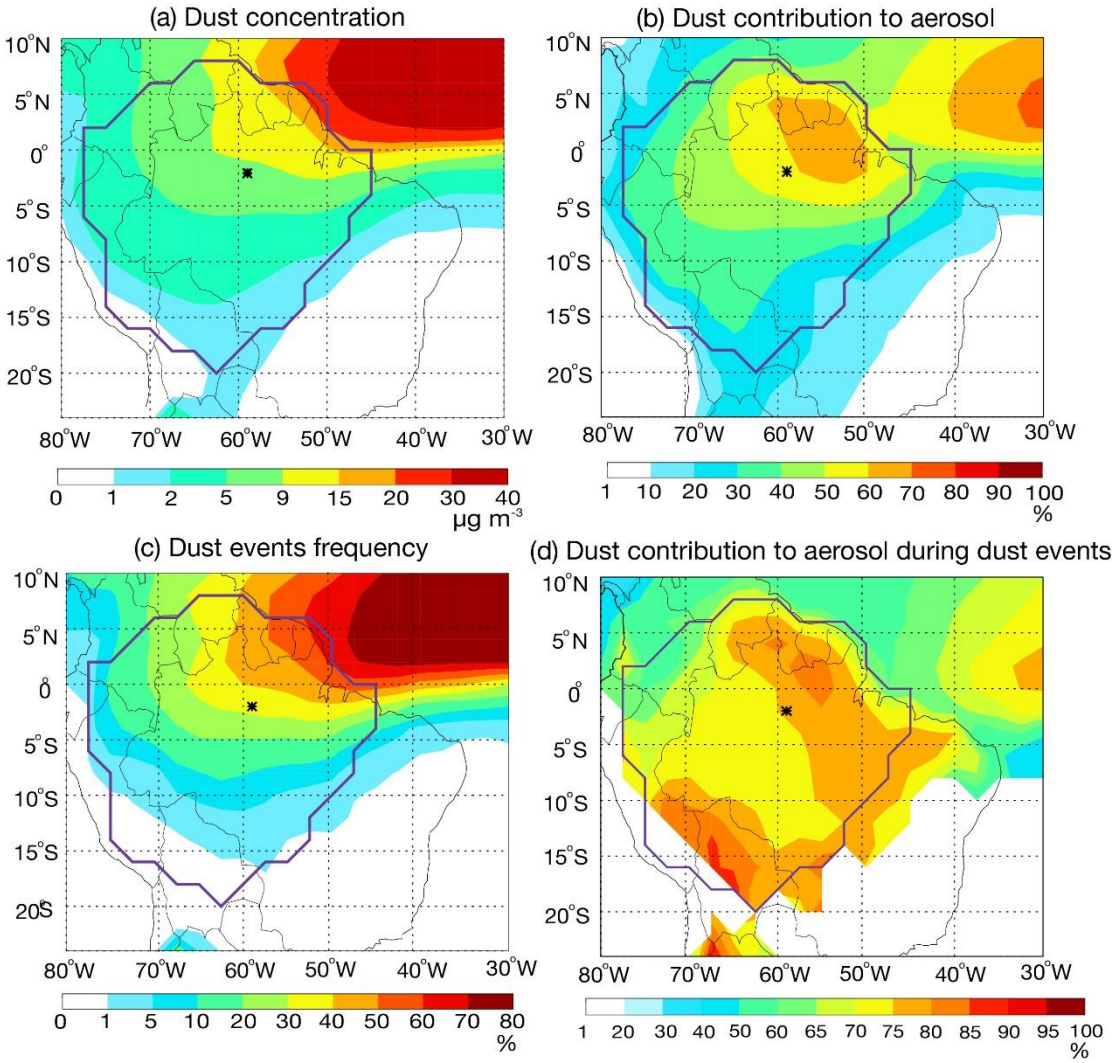

Figure 10. Dust impact over the Amazon Basin in the wet season of 2013 – 2017: (a) simulated surface dust concentrations, (b) dust contribution to surface aerosol concentrations, (c) the frequency of dust events, and (d) dust contribution to surface aerosol concentrations during dust events. The location of ATTO site is marked as asterisks. The region of Amazon Basin is marked by purple lines.

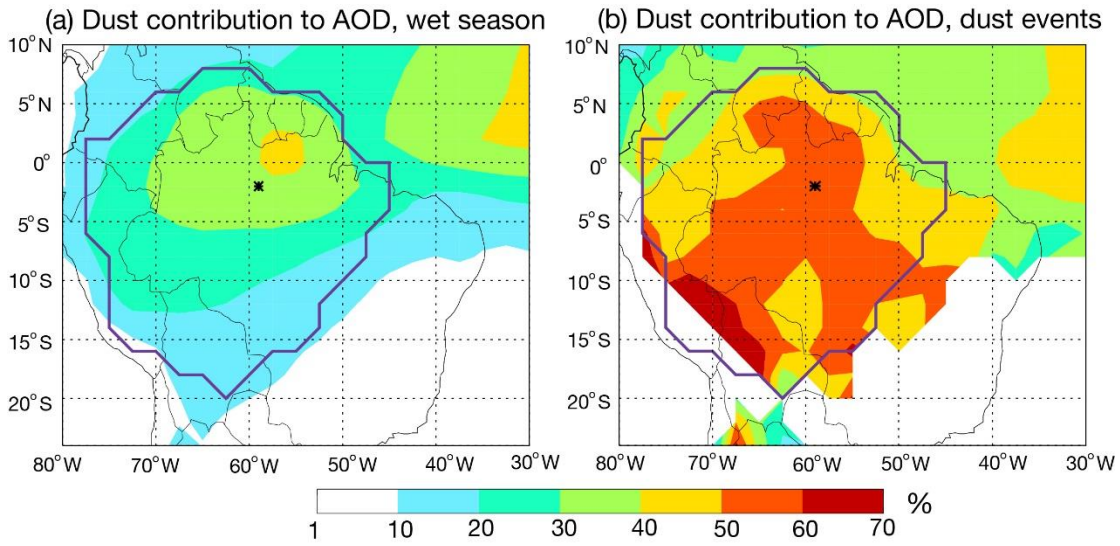

Figure 11. Dust contribution to total AOD at 550 nm over the Amazon Basin averaged over the (a) wet season and (b) dust events during 2013 – 2017. The region of Amazon Basin is marked by purple lines.

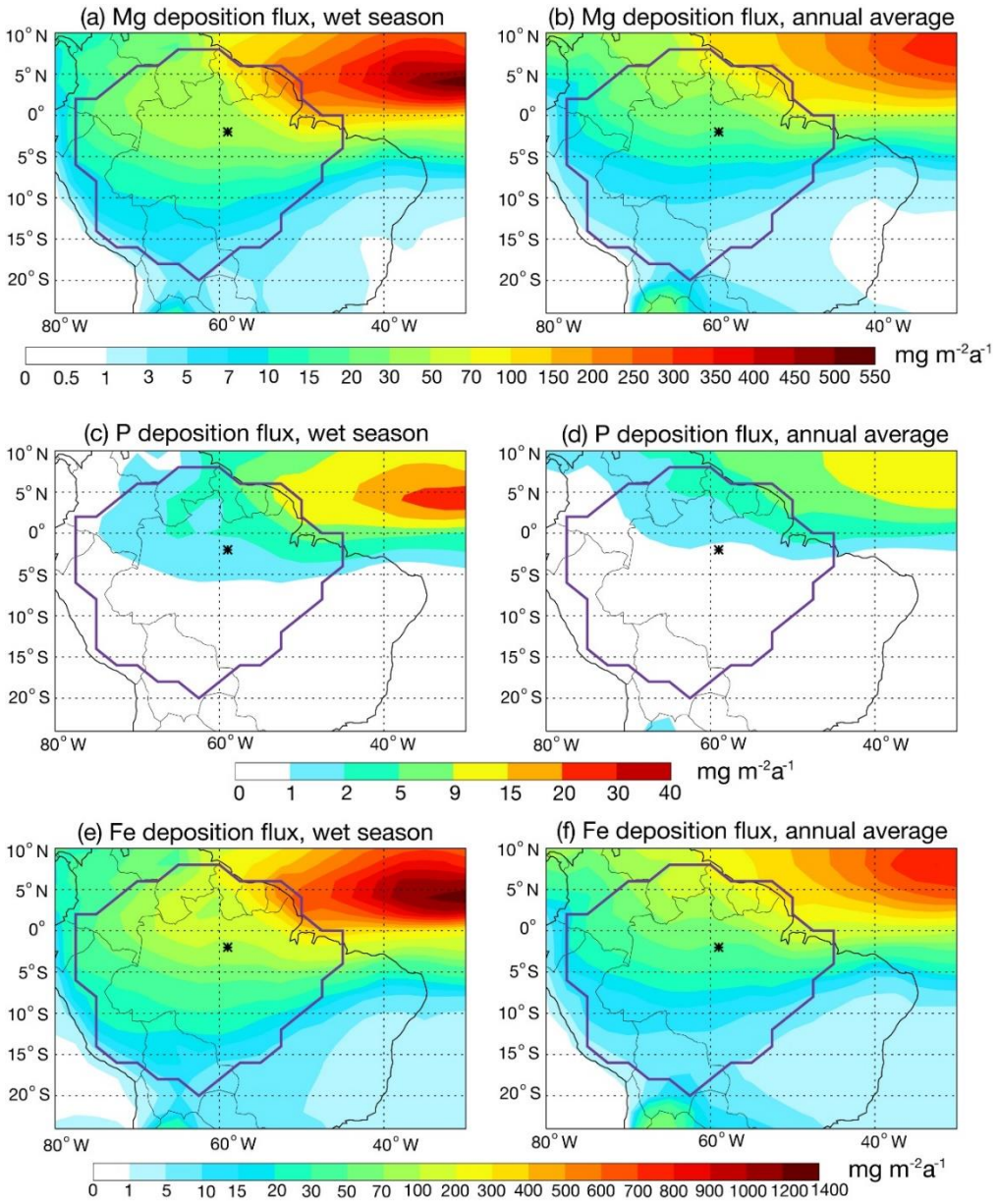

Figure 12. Magnesium deposition flux in (a) wet season and (b) annual averaged from 2013 to 2017. Phosphorus deposition flux in (c) wet season and (d) annual averaged from 2013 to 2017. Iron deposition flux in (e) wet season and (f) annual averaged from 2013 to 2017. The location of ATTO site is marked as asterisks. The region of Amazon Basin is marked by purple lines.